

DESIGN AND ANALYSIS OF INTEGRATED PLANAR TRANSFORMER
FOR LLC CONVERTER

by

Vigneshwaran Gurusamy



APPROVED BY SUPERVISORY COMMITTEE:

Dr. Bilal Akin, Chair

Dr. Murat Torlak

Dr. Ghanshyamsinh Gohil

Copyright 2018
Vigneshwaran Gurusamy
All Rights Reserved

To my beloved family

DESIGN AND ANALYSIS OF INTEGRATED PLANAR TRANSFORMER
FOR LLC CONVERTER

by

VIGNESHWARAN GURUSAMY, B. TECH

THESIS

Presented to the Faculty of
The University of Texas at Dallas
in Partial Fulfillment
of the Requirements
for the Degree of

MASTER OF SCIENCE IN
ELECTRICAL ENGINEERING

THE UNIVERSITY OF TEXAS AT DALLAS

May 2018

ACKNOWLEDGMENTS

I would like to express my sincere gratitude to my supervisor Dr.Bilal Akin for providing me an opportunity to work on this thesis. I am very fortunate to work under him due to his patience, consistent support and motivation. His method of approaching problems are very logical and pragmatic which inspired me to learn and improvise. I wish to thank my graduate committee members Dr.Murat Torlak and Dr.Ghanshyamsinh Gohil for accepting my request and providing their time to be part of the committee.

I also want to thank my friends and colleagues at Power Electronics and Drives Lab, Mohsen Zafarni, Kudra Baruti, Feyzullah Erturk, Enes Ugur, Syed Ali, Yuan Qi, Shi Pu, Chi Xu and Fei Yang for their help during several occasions. I am especially thankful to Dr.Emine Bostanci for her support in learning and working with Ansys Maxwell. My heartfelt gratitude towards her for helping me even after leaving UT Dallas. I am also thankful to GCI technologies for the project and especially Mr.Dean Gray and Mr.Javier Haro for their support.

My earnest gratitude to my parents and beloved family members for their continuous support and prayers during all the stages of my life. I am always thankful for their blessings which makes me to climb new heights. Last but not the least, I am thankful to my wonderful friends and roommates, Avinash Chandrasekharan, Barathkumar Rajasekar, Narayanan Padmanabhan and Varun Kumar Manohara Selvan for their moral support and preparing me delicious food whenever I need.

April 2018

DESIGN AND ANALYSIS OF INTEGRATED PLANAR TRANSFORMER FOR LLC CONVERTER

Vigneshwaran Gurusamy, MS
The University of Texas at Dallas, 2018

Supervising Professor: Dr.Bilal Akin

Planar Magnetics is replacing conventional magnetic structures in many applications. Especially Planar transformers are good choice for applications requiring integrated magnetics. LLC converter takes advantage of the features of planar magnetics resulting in power density improvement of the converter system. This thesis deals with design of one such integrated planar transformer for LLC converter. Design flow of integrated planar magnetics is discussed in detail. The major issue of high frequency eddy current loss and achieving required leakage inductance are highlighted. The reason behind the high frequency eddy current losses due to proximity effect and skin effect are discussed and solution to address the high frequency loss are provide. It is shown that the solutions to reduce eddy current losses reduces leakage inductance which is good for converter systems where only magnetizing inductance of transformer plays vital role and the leakage inductance, a parasitic parameter causes undesired effects. For integrated transformer where we need significant leakage inductance, modifying design to include a leakage layer is shown to improve leakage without compromising losses.

TABLE OF CONTENTS

ACKNOWLEDGEMENTS	v
ABSTRACT	vi
LIST OF FIGURES	x
LIST OF TABLES	xii
CHAPTER 1 Introduction	1
1.1 Review of planar magnetics technology	1
1.1.1 Advantages of planar magnetic technology	2
1.1.2 Limitations of planar magnetic technology	4
1.1.3 Planar magnetic core	4
1.1.4 Planar windings	7
1.2 Magnetic integration	9
1.3 Introduction of LLC converter	12
1.3.1 Resonant converters	12
1.3.2 Resonant converter topologies	13
1.3.3 ZCS and ZVS region in resonant converter	15
1.3.4 LLC resonant converter	16
1.4 Magnetics for LLC converter	19
1.4.1 Discrete magnetics for LLC converter	20
1.4.2 Integrated magnetics for LLC converter	20
1.4.3 Conventional magnetic integration	20
1.4.4 Leakage inductance as resonant inductor	21
1.5 Thesis organization	23
CHAPTER 2 DESIGN EQUATIONS OF TRANSFORMER	25
2.1 Introduction	25
2.2 Design equations	25
2.2.1 Area product	27
2.2.2 Determination of airgap	27
2.2.3 Thermal considerations	29

2.2.4 Determination of winding parameters	31
2.3 Loss calculation	33
2.3.1 Core loss calculation	33
2.3.2 High frequency eddy current loss calculation.....	34
2.4 Calculation of leakage inductance	35
CHAPTER 3 DESIGN OF INTEGRATED PLANAR TRANSFORMER.....	36
3.1 Design specifications	36
3.2 Design results.....	37
3.3 Numerical modeling of transformer.....	41
3.3.1 Electromagnetic finite element analysis	41
3.3.2 Eddy current solver	42
3.3.3 Computation of magnetizing and leakage inductance	43
3.3.4 Simulation results.....	45
CHAPTER 4 HIGH FREQUENCY EDDY CURRENT LOSS STUDY	47
4.1 Introduction.....	47
4.2 Skin effect	47
4.3 Proximity effect	50
4.3.1 MMF in a current carrying conductor.....	52
4.3.2 MMF in transformer windings.....	53
4.4 Reduction of copper loss due to proximity effect.....	54
4.4.1 Interleaved windings.....	54
4.4.2 Conductor thickness variation study.....	57
CHAPTER 5 IMPROVEMENT OF LEAKAGE INDUCTANCE	59
5.1 Introduction.....	59
5.2 Methods to calculate leakage inductance.....	60
5.2.1 Energy storage method	60
5.3 Methods to improve leakage inductance.....	61
5.3.1 Ampere turn of winding.....	61
5.3.2 Winding and insulation geometry	61
5.3.2 Leakage layer	62
5.4 Design with magnetic leakage layer	62

5.4.1 Magnetic reluctance model of transformer	63
5.5 New design with reduced ampere turns	69
5.6 Magnetic shunt in new design.....	72
CHAPTER 6 CONCLUSION AND FUTURE WORK	78
6.1 Summary	78
6.2 Future work	79
REFERENCES	80
BIOGRAPHICAL SKETCH.....	84
CURRICULUM VITAE	

LIST OF FIGURES

Figure 1.1 Typical conventional transformer.....	2
Figure 1.2 Typical planar transformer	2
Figure 1.3 Hysteresis loop of soft ferrite	5
Figure 1.4 Typical PCB winding	8
Figure 1.5 Typical flat copper winding.....	9
Figure 1.6 Two discrete inductors	10
Figure 1.7 Integrated inductor with decoupled flux.....	11
Figure 1.8 Integrated inductor with coupled flux	11
Figure 1.9 Series resonant tank.....	13
Figure 1.10 Parallel resonant tank	14
Figure 1.11 Series parallel resonant tank.....	15
Figure 1.12 LLC resonant tank	15
Figure 1.13 Typical DC characteristics of resonant converter	16
Figure 1.14 Schematic of full bridge LLC resonant converter	17
Figure 1.15 Typical DC gain characteristics of LLC resonant converter	18
Figure 1.16 Conventional integration of an inductor and a transformer.....	21
Figure 1.17 Equivalent circuit of transformer.....	22
Figure 1.18 Equivalent circuit of transformer referred to primary side.....	22
Figure 2.1 B-H curve of a magnetic core with and without airgap.....	28
Figure 2.2 Simple core with an airgap	30
Figure 2.3 Conductor with rectangular cross section.....	33
Figure 3.1 Planar PCB winding	39
Figure 3.2 Loss data characteristics curve	39
Figure 3.3 Structural arrangement of transformer	40
Figure 4.1 Skin effect in round conductor	48
Figure 4.2 Variation of skin depth vs frequency.....	49
Figure 4.3 Skin effect in rectangular section conductor	49
Figure 4.4 Proximity effect in round conductor.....	50
Figure 4.5 Proximity effect in rectangular section conductor.....	51

Figure 4.6 MMF across a conductor with uniform current density	52
Figure 4.7 MMF in a transformer with multiple layer windings	53
Figure 4.8 MMF in initial design without interleaving.....	54
Figure 4.9 Sectional view of partially interleaved structure	55
Figure 4.10 MMF in partially interleaved structure.....	55
Figure 4.11 Sectional view of fully interleaved structure	56
Figure 4.12 MMF in fully interleaved structure	56
Figure 4.13 Copper loss vs PCB thickness	58
Figure 5.1 Leakage flux	59
Figure 5.2 Transformer with leakage layer	62
Figure 5.3 Transformer reluctance model.....	64
Figure 5.4 Leakage inductance vs airgap length for different shunt thickness.....	65
Figure 5.5 Magnetizing inductance vs shunt thickness for different airgap length	66
Figure 5.6 Magnetizing inductance vs airgap length for different permeability	67
Figure 5.7 Leakage inductance vs airgap length for different permeability	68
Figure 5.8 New design result	70
Figure 5.9 2D FEA model.....	71
Figure 5.10 Partially interleaved FE model	72
Figure 5.11 Conductor thickness verification.....	73
Figure 5.12 Magnetizing inductance for permeability (a)100,(b)150,(c)200 and (d)250.....	75
Figure 5.13 Leakage inductance at various permeability	76
Figure 5.14 Copper loss vs shunt thickness at various permeability	76

LIST OF TABLES

Table 1.1 Standard planar core data [7]	6
Table 1.2 Comparison between conventional E-core and equivalent planar E-core [5]	7
Table 3.1 Design specifications for integrated transformer.....	36
Table 3.2 Geometrical parameters of selected ER core	38
Table 3.3 Design result comparison.....	45
Table 4.1 Simulation result of different winding structure	57
Table 5.1 Geometrical parameters of selected EE core	69
Table 5.2 Design result comparison.....	71
Table 5.3 Partially interleaved winding design result comparison	72
Table 5.4 Final design result comparison	77

CHAPTER 1

INTRODUCTION

1.1 Review of planar magnetics technology

Improvement of power density and efficiency of power conversion systems has been a research focus for many years. Size of magnetic components and thermal management of system mainly limits power density of such power electronic system. It is well-known that the increase in switching frequency yields significant improvement in power density as it facilitates the size miniaturization of magnetic components. If we consider the switching loss in power devices are taken care of, this comes with difficulty in achieving efficient magnetic components with conventional magnetic technology. This is due to the eddy current and proximity effect loss faced by the standard circular conductors are more pronounced at frequencies higher than 100 kHz [2].

The Planar Magnetic technology has received attention since last decade as it paved way to improve power density of power electronic converters. One of the early research work on planar technology was published by Alex Estrov in 1986. Since then a lot of research activities has been performed on this magnetics technology [1]. The typical structure of a conventional transformer and a planar transformer are shown in Figure 1.1 and 1.2 respectively. The size of the planar magnetic component is smaller in height (z-axis) and has more surface area than the conventional magnetic component. The planar windings are stacked on top of one another in z-axis whereas the conventional windings are wound around the core in a way similar to low frequency power transformer. These differences in core geometry and winding provides edge over the conventional technology in multiple factors like power density, ease of manufacturing and repeatability of parameters of magnetic device.

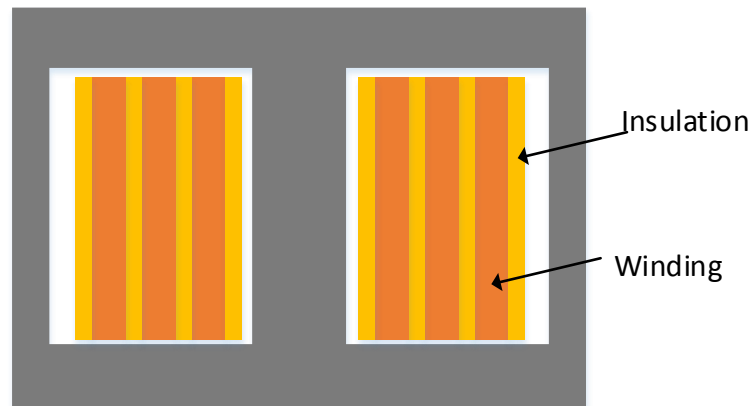


Figure 1.1 Typical conventional transformer

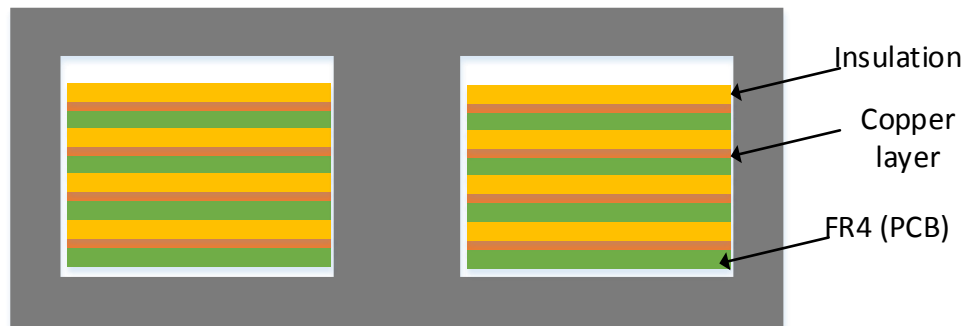


Figure 1.2 Typical planar transformer

1.1.1 Advantages of planar technology

This technology offers numerous advantages over conventional technology which are discussed as follows

1. Low profile design

Low profile over conventional structures due to more surface area of design with reduced cubic volume. This provides higher volumetric efficiency.

2. Ease of manufacturing

As windings are made with PCB or stamped copper sheets, the assembly process is made easy with the computer aided manufacturing whereas the conventional winding is difficult to automate [3].

3. Reduced AC conduction loss

Winding structure used in planar technology tends to have lesser AC resistance than equivalent round wire winding. In [4], based on the analysis of different windings, it has shown that the PCB and foil windings have reduced resistance than solid winding but higher than litz winding.

4. Controlled leakage inductance

Leakage inductance of the transformer depends on the relative position of primary and secondary winding in the core of planar transformer. As the winding position and gap between the windings are strictly controlled, the leakage inductance is also tightly controlled.

5. High power density

As the surface area to volume ratio of planar magnetic components are significantly higher than conventional structure, conduction of heat is improved. This results in better cooling which facilitates higher power for same temperature increase thereby improved power density.

6. Good repeatability of parameters

As the planar magnetic structure is tightly controlled, the windings and insulators are located precisely. This provides better controlled and consistent parasitic parameters. This is in contrast to wire wound magnetics which are prone to variation from operator to operator as they do not have tight control over layout of winding.

1.1.2 Limitations of planar technology

The component size reduction is achieved with the help of microelectronic processing. Though this magnetic technology has more advantages it also suffers from some limitations.

1. Increased footprint area

Due to the increase in surface area of the core, the footprint area of the component is more than equivalent conventional magnetic component.

2. Reduced window area

On comparing cores of similar size in Table 1.2 [5], the window area of planar core is much lesser than the traditional counterpart. This provides less room for copper windings.

3. Low copper fill

In most of planar magnetic components PCB based windings are used which has low copper fill factor about 0.25 whereas traditional method has about 0.4. This is due to the fact that the winding in PCB has higher inter turn spacing and dielectric thickness [2]

1.1.3 Planar magnetic core

Magnetic cores are made of soft magnetic materials. These materials can achieve high flux density with less coercive force in contrast to hard magnetic materials which are used commonly in permanent magnets. They have less hysteresis loop area as shown in Fig.1.3 which attributes to reduced hysteresis loss. There are different types of core materials like soft ferrites, powdered iron core, amorphous alloys, nanocrystalline materials etc. But most of the planar cores are made of soft ferrites due to their reduced core loss.

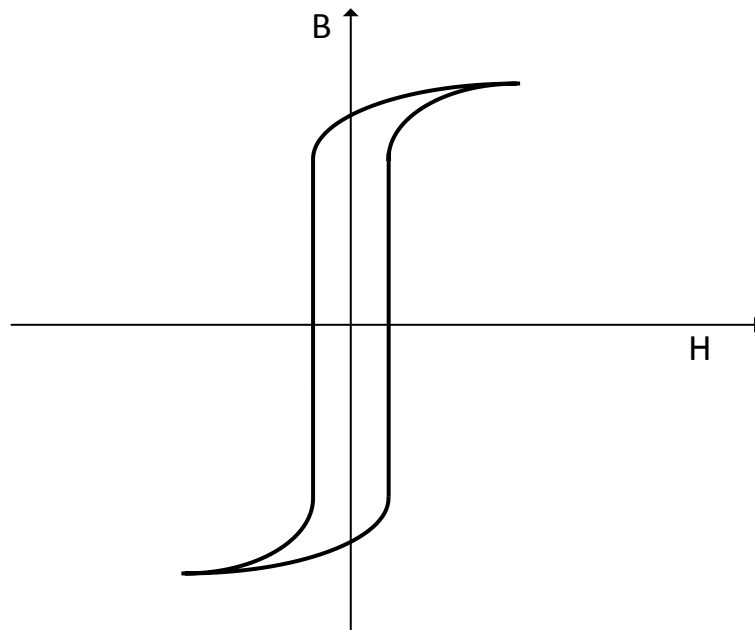


Figure 1.3 Hysteresis loop of soft ferrite

Ferrites are made of iron oxide and alloyed with metals like cobalt, magnesium, nickel, silicon, manganese, or zinc. The most commonly used ferrites are manganese-zinc (Mn-Zn) and nickel-zinc (Ni-Zn). Ni-Zn ferrites have high electrical resistivity and less permeability. It is used for high frequency applications generally in order of MHz. Mn-Zn ferrites have reduced electrical resistivity and higher permeability than Ni-Zn ferrites. It is used in applications where frequency is in the order of few hundreds of kHz. Its real part of complex permeability which is responsible for energy storage begins to fall off at about 1MHz [6]. Some of the issues with the ferrites are brittleness and low Curie temperature which has to be appropriately considered during design.

There are different planar core types like EI, ER, EE, EQ and PQ are available from manufacturers. The cores with circular center pole like ER, PQ and EQ cores have reduced Mean Length Turn (MLT) due to window shape which results in reduced resistance and thereby loss. The size of the component also reduces than equivalent design with another core like EE as it the

winding has to be extended out of the core. Some standard planar core details from Ferroxcube planar cores are shown in Table 1.1. Dimension represents the external size of the core. Area product is the product of window area and cross-sectional area of the core. Higher the area product higher is its power handling capacity.

Table 1.1 Standard planar core data [7]

Core type		Model	Dimension (mm)	Area product (mm ³)	Weight (g)
EE	Min	EE14	14*5*7	200	1.2
	Max	EE64	64*50.8*20.4	115000	200
ER	Min	ER95	9.5*5*4.9	23.7	0.7
	Max	ER64	64*50.8*25.4	99616	304
EQ	Min	EQ13	12.8*8.7*5.7	69.6	1.6
	Max	EQ38	38.1*25.4*16	4334	43
PQ	Min	PQ20/16	21.3*14*16.2	1450	13
	Max	PQ50/50	51*32*50	98400	195

From the above table, it can be seen EE core has higher area product per size and weight. ER core has the smallest size of all. EQ core has limited maximum size. PQ planar core does not look like low profile as the height and length of max size is almost same.

The Table 1.2 compares a planar E-core with an equivalent conventional E-core. Window area of planar core is much smaller and even smaller than the core cross sectional area. Due to the small window, windings have to be used efficiently with the help of higher flux density than

conventional core. Though the area product and volume of planar are lesser than the conventional core, it can be designed for similar specifications. This gives advantage of reduced size and weight. As the surface area of planar core is higher, it has better thermal performance than the conventional core.

Table 1.2 Comparison between conventional E-core and equivalent planar E-core [5]

Magnetic technology	Planar	Conventional
Core type	E/E32	E2627
Total window area	0.605 cm ²	1.127 cm ²
Core cross sectional area	1.29 cm ²	0.836 cm ²
Area Product	0.78 cm ⁴	0.94 cm ⁴
Exposed surface area	23 cm ²	19 cm ²
Minimum Height	13 mm	25 mm

1.1.4 Planar windings

The type of the winding used for a planar structure is determined by window area of the core, frequency of operation, manufacturing cost and application. The size of the conductor is determined by the current density and switching frequency. The different types of winding methods available for planar magnetics are PCB windings, flat copper foil winding, flex winding, ribbon winding, Low temperature co-fired ceramic (LTCC), etc. Among these most popular technologies are PCB windings, flat copper foil and flex windings.

1. PCB winding

The printed circuit board windings are formed by copper cladded PCB. The two sided boards

are normally used with copper thickness of 4oz – 8 oz and substrate thickness of about 450 μ m. This allows easy connection of layers in a multiple layer winding. It facilitates easy interleaving of windings which is difficult in a conventional transformer. It has advantages of easy assembly process, low cost manufacturing in high volume and high surface area of windings needed for high frequency application [8]. A typical PCB winding is shown in Fig.1.4

PCB windings facilitate the integration of winding of magnetics in PCB of converter itself. Currently it is limited to low power applications. The major disadvantage of this winding technology is the reduced copper fill due to high area of substrate. It also faces hotspot issues due to holes created for connection in multilayer PCB [9].

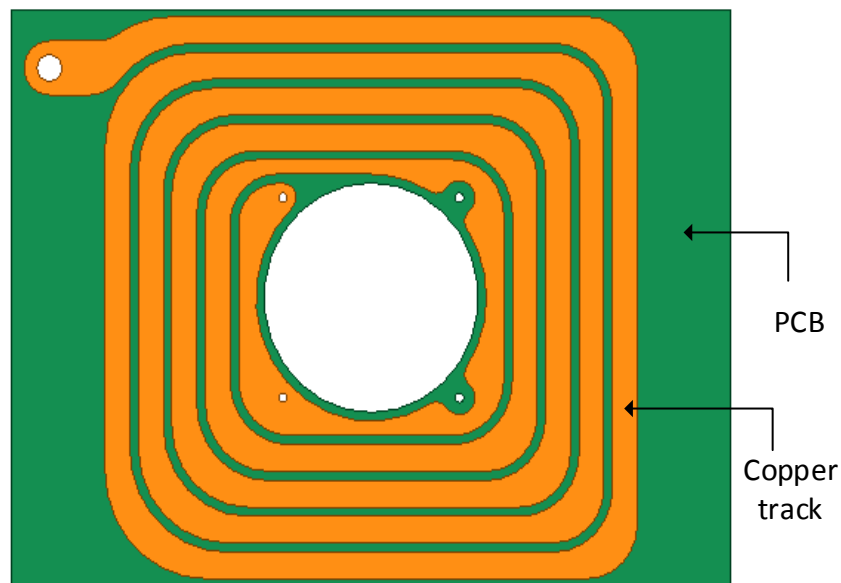


Figure 1.4 Typical PCB winding

2. Flat copper winding

These are bare copper sheets fabricated to form winding. Normally used lesser turns with high planar area. The major limitation is proper insulation of winding and aligning them properly.

A typical flat copper winding is shown in Fig.1.5



Figure 1.5 Typical flat copper winding

3. Flex winding

Flex circuit uses a dielectric layer of thickness as low as 50 μm which is smaller than PCB dielectric. The windings can be fabricated similar to PCB winding with higher utilization of window area.

1.2 Magnetic integration

Magnetic integration is the technique in which multiple magnetic components are fabricated in a single magnetic structure. The magnetic components can be inductors or inductor and transformer. Integrated magnetics design has been in the realm of research for quite a long time.

It is demonstrated in [10] that it is possible to integrate discrete transformer and inductors of any switching power converter.

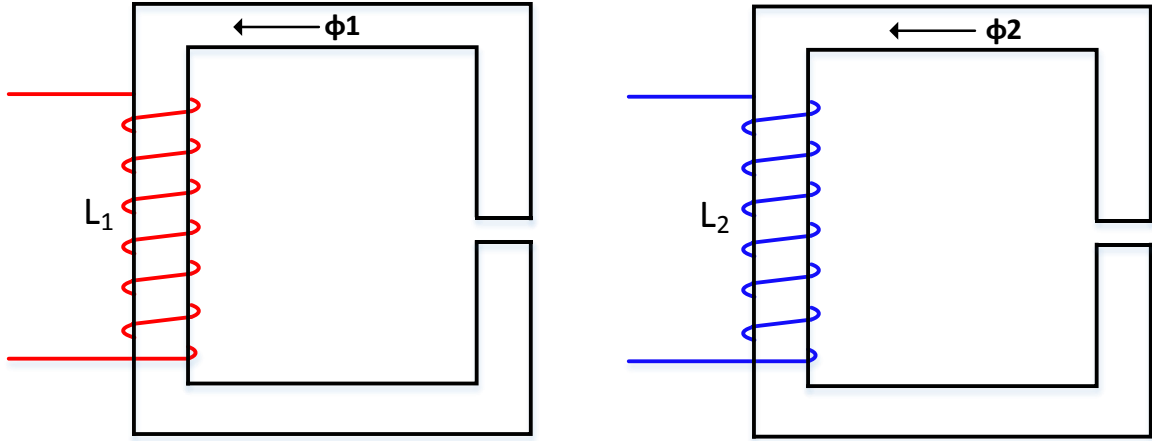


Figure 1.6 Two discrete inductors

To illustrate magnetic integration, simple example with two discrete inductors are taken. The discrete inductors with core are shown in Fig.1.6. The cores of the inductors are integrated which means both the inductor windings are placed in the single magnetic core. The integrated structure is shown in Fig.1.7. The central limb cross section can be reduced with the appropriate design of magnetics. This leads to significant size reduction. Here there exists flux decoupling between inductors.

In the magnetic structure shown in Fig.1.8, the central limb is removed which results in flux coupling between the inductors. The effective core area should be appropriately selected to prevent core saturation during the operation. This type of structure normally use the core which facilitates winding in all of its legs like EE and EI cores. The proper implementation of integrated magnetics

results in significant weight, size and cost reduction of the converter system. The reduction core size leads to reduced core losses as both eddy current and hysteresis loss depends on the volume of core. This also leads to improvement in efficiency. With the current ripple reduction, switching frequency can be decreased to reduce switching losses.

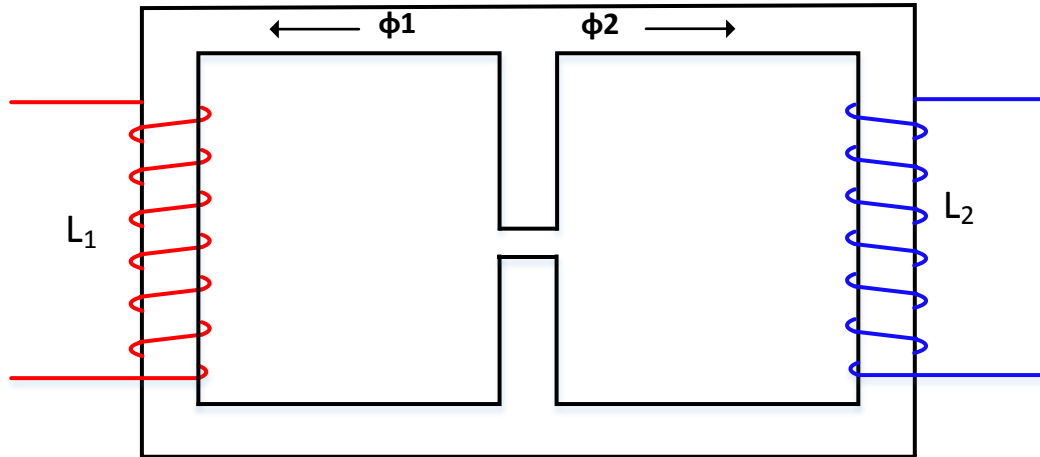


Figure 1.7 Integrated inductor with decoupled flux

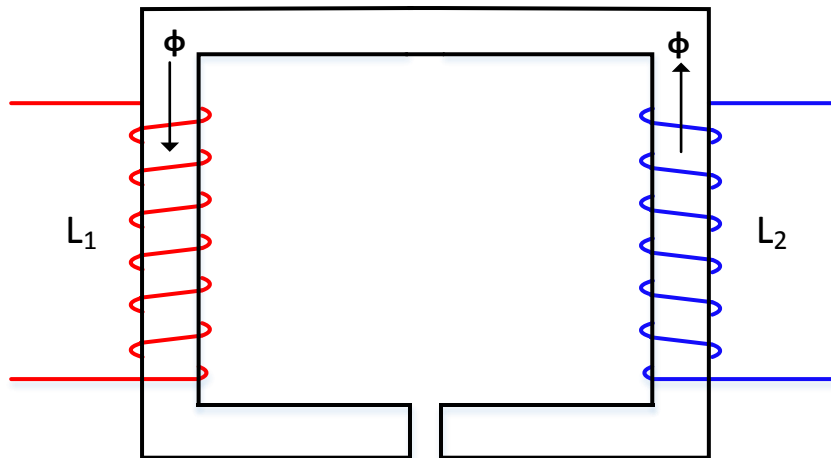


Figure 1.8 Integrated inductor with coupled flux

The magnetic integration can also be implemented in resonant converters which helps to reduce voltage stress on switching devices [13]. This kind of integration can be done with planar

magnetic structure resulting in low profile design. A new geometry of integrated inductors are proposed with 3 planar I cores in [14] for a bi-directional DC-DC converter.

The design of integrated magnetics is difficult than discrete magnetics. When designing decoupled inductors, flux distribution in the core may not be uniform. To overcome this, different air gaps can be used in the legs which increases manufacturing complexity. The core of integrated magnetic component is usually bigger than the discrete structure. The integrated magnetic is sensitive to parasitics which can be limited by using planar structure. There are still limitations with planar magnetic integration as the distribution of windings in outer legs increases the size of structure and has less control over the magnetic leakage.

1.3 Introduction to LLC converter

LLC converter comes under the family of resonant converters. The resonant converters are introduced briefly first in this section.

1.3.1 Resonant converters

In PWM converters, state transition of power devices occur by abruptly interrupting power flow in the device. This is termed as hard switching. This causes significant power loss, voltage spikes resulting in device stress. Resonant converters achieve low switching losses which enable them to operate at high switching frequency. This is achieved with the help of soft switching of semiconductor devices. The term soft switching means switch transition occurs when either current through the switch or voltage across the switch are zero. Thus, there are two commutation scheme namely zero voltage switching (ZVS) or zero current switching (ZCS). In ZVS, the voltage across

the device is made zero or close to zero during the transition of state of switch. In ZCS, current through the device is made zero during the transition. This technique reduces switching losses and stress experienced by the devices. It has some issues, resonant converters are controlled by frequency of operation rather than the pulse width in PWM converters. This increases the complexity of control [15]. The other issue is the circulating current in resonant circuitry which leads to increased conduction loss [16].

1.3.2 Resonant converter topologies

There are different topologies in resonant converters. Some of the popular topologies are Series Resonant Converter, parallel resonant converter, series parallel resonant converter and LLC resonant converter.

In *series resonant converter*, resonating elements L and C are connected in series with the load and the resonant tank is shown in Fig 1.9. The resonant tank and load forms a voltage divider network. By controlling switching frequency, the impedance of resonant tank is controlled which in turn controls voltage across the load. The maximum gain is achieved at resonant frequency where the impedance of resonant tank is very low. When operating frequency is away from resonant frequency, there will be more circulating current in resonant current leading to higher conduction losses. Some of the issues with this converter are difficulty in regulation at light load condition, high circulating current and high turn off current at high input voltage.



Figure 1.9 Series resonant tank

In *parallel resonant converter*, the resonating elements are connected in series whereas load the load is connected in parallel to the resonant tank. The resonant tank structure is shown in Fig.1.10. The load is connected across the resonant capacitor. The maximum gain is achieved at resonant frequency when converter is operated away from resonant frequency there will be significant circulating current in resonant tank. During the light load condition, the regulation can be achieved due to its narrow operating region, but the issue is circulating current even at resonance as the impedance of tank is very small. When there exists wide variation in input voltage, it also has issue of high turn off current at high input voltage.

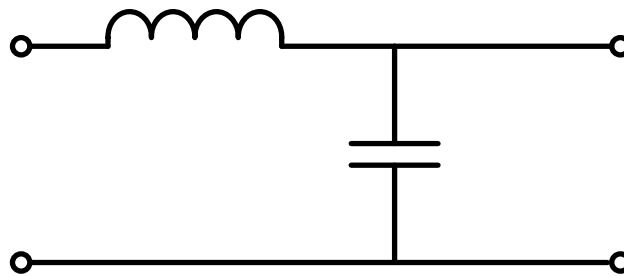


Figure 1.10 Parallel resonant tank

The *series parallel resonant converter* has three passive elements, one L and two C. It is also called as LCC converter. L and C forms a series resonant tank which is connected in series with the load. The tank structure is shown in Fig.1.11. The other capacitor is connected in parallel to the load. The series tank works in same way as series resonant converter with less circulating current than parallel resonant converter. The parallel capacitor helps in achieving regulation at light load condition. This topology also has high losses during turn off at high input voltage. This makes the switching loss at high input voltage similar to a PWM converter.

LLC Converter is duality of LCC resonant converter. This makes the resonant tank dual network of LCC. The resonant tank of LLC converter is shown in Fig.1.12.

The advantages of LLC converter over other resonant topologies and its operation are discussed in following sections.

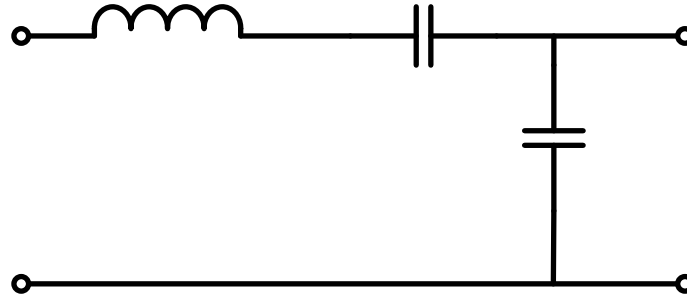


Figure 1.11 Series parallel (LCC) resonant tank

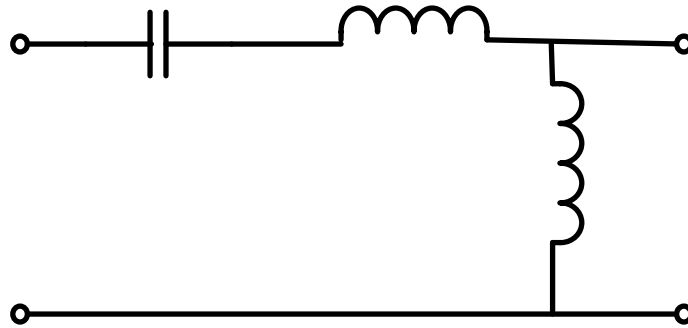


Figure 1.12 LLC resonant tank

1.3.3 ZCS and ZVS region in a resonant converter

Resonant converters achieve soft switching with the help of inductors and capacitors tuned to resonance at operating frequency. Due to resonance, there exists zero crossing of voltage and current which facilitates soft switching. The Fig.1.13 shows typical DC characteristics of a resonant converter. The positive slope region is called capacitive region and negative slope region is called inductive region. Generally, all resonant converters achieve zero voltage switching when operating in inductive region [17]. The operation in capacitive region has to be prevented since

current leads voltage which will cause the current to reverse before switching device turns off. This will result in conduction of antiparallel diode and hard commutation of diode occurs when the other device in the bridge turns on causing reverse recovery losses.

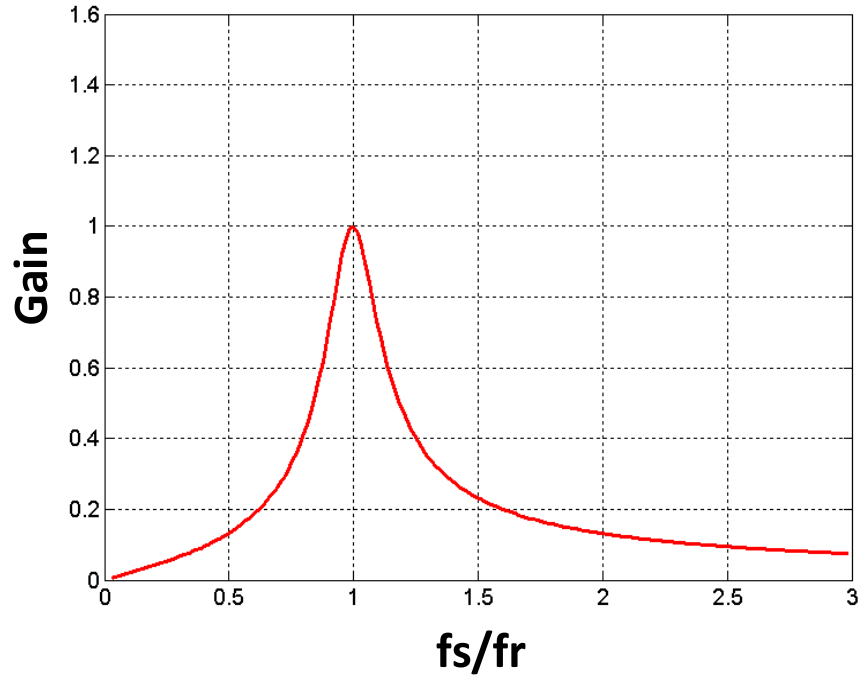


Figure 1.13 Typical DC characteristics of a resonant converter

The efficiency of converter will be high when operated at resonant frequency. Both LCC and LLC has two resonant frequencies. But the lowest resonant frequency of LCC converter is in ZCS region. By bringing the resonant frequency in ZCS region to ZVS region, the efficiency of the converter can be improved. This is achieved with LLC resonant converter.

1.3.4 LLC resonant converter

All the resonant topologies discussed in previous section suffers from high turn off loss during high input voltage. Basically they could not achieve soft switching for wide range of input

voltage. LLC converters has benefit of achieving ZVS even at no load condition and operating at narrow frequency range in light load condition.

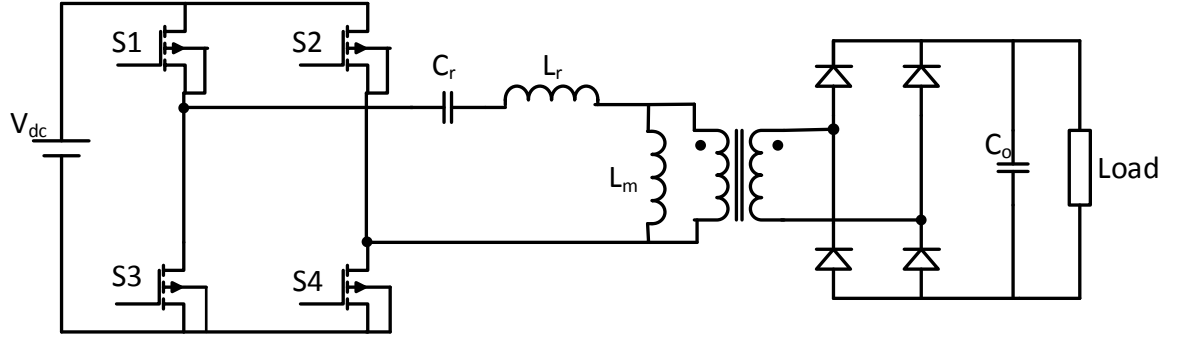


Figure 1.14 Schematic of full bridge LLC resonant converter

The schematic of a full bridge LLC resonant converter is shown in Fig.1.14. The MOSFET H-bridge generates square wave voltage which is applied as input to resonant network. Typically, duty ratio is fixed at 0.5 which makes both the half cycle symmetrical. The resonant network consists of two inductors and capacitor. Due to resonance nature, only the fundamental component of applied square wave voltage involves in power transfer which makes the current sinusoidal. Due to the inductive region of operation, the current lags voltage. This allows the switches to be turned off at zero voltage thereby achieving ZVS. The ac voltage is rectified with a diode bridge rectifier circuit.

The DC gain characteristics of LLC converter is shown in Fig.1.15 which shows the ZCS and ZVS region of converter. There are two resonant frequencies for this converter. It can be seen that as load increases the resonant frequency increases. The resonant frequencies are given by

$$f_{res1} = \frac{1}{2\pi\sqrt{L_r * C_r}}$$

$$f_{res2} = \frac{1}{2\pi\sqrt{(L_m + L_r)*C_r}}$$

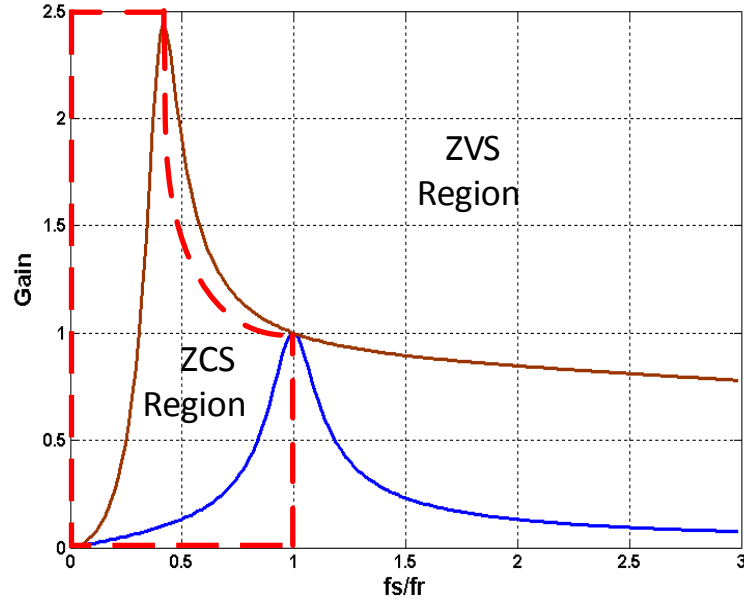


Figure 1.15 Typical DC gain characteristics of LLC converter

There are three modes of operation. The mode of operation varies based on the input voltage and output current. They are discussed as follows

1. Operation at resonance frequency, $f_s = f_r$

In this mode, the switching period is equal to the resonant period. The converter delivers output during both the half cycle. The resonant current wave shape is almost sinusoidal. At the end of every half cycle, resonant current reaches the magnetizing current and diode current reaches zero. This ensures ZVS of switches and soft commutation of diodes. The conduction losses are low in this frequency and efficiency of the converter is high. The gain characteristics in this mode of operation is unity. Generally, this is the operating frequency at rated input and output voltages.

2. Operation at $f_r < f_s < f_{r1}$

In this mode, the switching period is longer than resonant period. The output power is delivered till resonant period in both the half cycle. During the remaining switching period of half cycle, freewheeling operation occurs, and diode current becomes zero. ZVS of power switches and soft commutation of diode occurs. But the conduction losses are high due to circulating current during freewheeling. The gain characteristics in this mode of operation is greater than unity.

3. Operation at $f_s > f_{r1}$

In this mode, the switching period is shorter than resonant period. The power switch turns off before completion of resonant period which results in hard commutation during turn off. The power is delivered to load during switch transition which results in reverse recovery loss in diodes. This mode has least efficiency of all due to turn off and diode losses. The gain characteristics in this mode of operation is lesser than unity.

From the operation of converter, it is clearly seen the resonant frequency is the deciding criteria for processing power. The losses in the converter also varies based on how far or closer the switching frequency is from resonant frequency. This shows the importance of magnetic elements which determines the resonant frequency.

1.4 Magnetics for LLC converter

The magnetic elements required for LLC converter are two inductors and a transformer. Generally, one of the inductor is implemented with the magnetizing inductance of transformer. This brings down the required magnetics to an inductor and transformer with specific magnetizing inductance. This can be implemented in multiple ways. A separate inductor for resonant inductor

and a transformer. This is referred as discrete magnetics. The inductor can be fabricated along with the transformer in a single core. The integration of inductor and transformer in a single magnetic component is referred as integrated magnetics.

1.4.1 Discrete magnetics for LLC converter

This is typical magnetic structure which was in use for very long time. It has an inductor in a separate magnetic core and transformer in a separate magnetic core. This method is preferred only when the resonant inductor could not be integrated within transformer when the resonant inductance value is significantly high. Some of the issues with this design are two separate magnetic cores are needed, less reliability, more footprint area.

1.4.2 Integrated magnetics for LLC converter

This is more preferred magnetic design for LLC converter due to multiple magnetic components. Integration can be done in multiple ways. The windings of transformer and inductor can be fabricated in a single magnetic core. Then they are connected externally to form required connection. This is conventional method of integration. The other method is to utilize the leakage inductance of transformer as resonant inductor. Both the type of integration are discussed in the following section.

1.4.3 Conventional integration:

Magnetic integration indicates combining one or more magnetic elements within in a single magnetic structure. Instead of having two separate magnetic cores for inductor and transformer,

both are placed in a single core as shown in Fig.1.16. Some of the advantages of this type of integration are reduction in magnetic component count and scope for reduction in footprint by optimizing the design. It is difficult to achieve magnetic decoupling between the components. Some of the disadvantages are the temperature may increase if cooling is not improved, copper losses in magnetic structure may remain same or even increase due to increase in temperature, possibility for increase in EMI as the leakage need not be confined within magnetic structure.

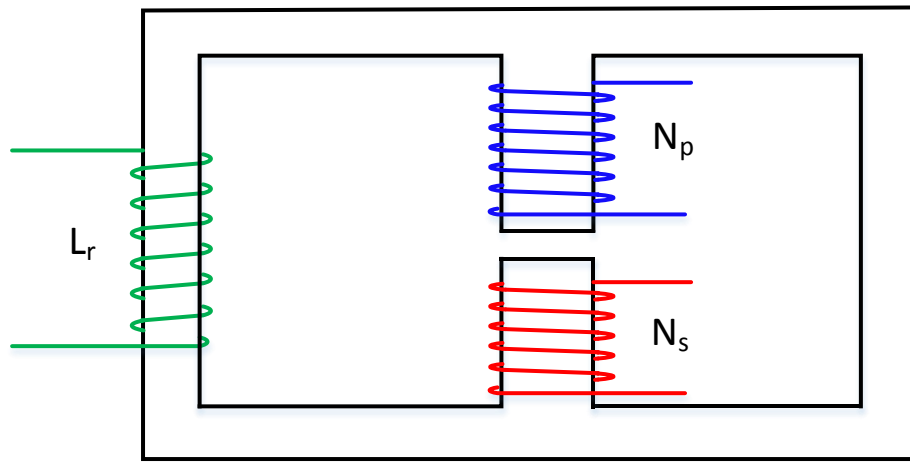


Figure 1.16 Conventional integration of an inductor and a transformer

1.4.4 Leakage inductance as resonant inductor:

The equivalent circuit of transformer neglecting core loss is shown in Fig.1.17. It can be seen there is a series inductance connected with magnetizing inductance of transformer. This is leakage inductance of transformer in primary side. The secondary side of the transformer also has inductance in series with the load. The equivalent circuit of transformer with secondary side referred to primary is shown in Figure1.18. This is the total leakage inductance of the transformer. This leakage inductance can be used as resonant inductor for LLC converter which is given by

$$L_{lk} = L_{lk1} + L_{lk2} \left(\frac{N_2}{N_1} \right)^2 \quad (1.1)$$

N_1 – number of turns in primary winding of transformer

N_2 – number of turns in secondary winding of transformer

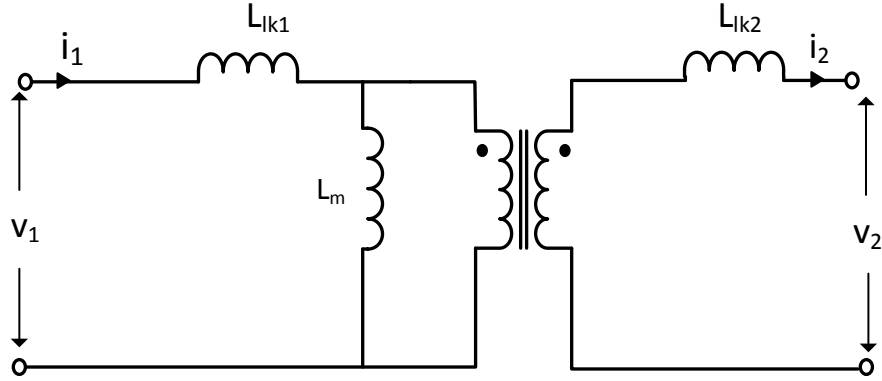


Figure 1.17 Equivalent circuit of a transformer

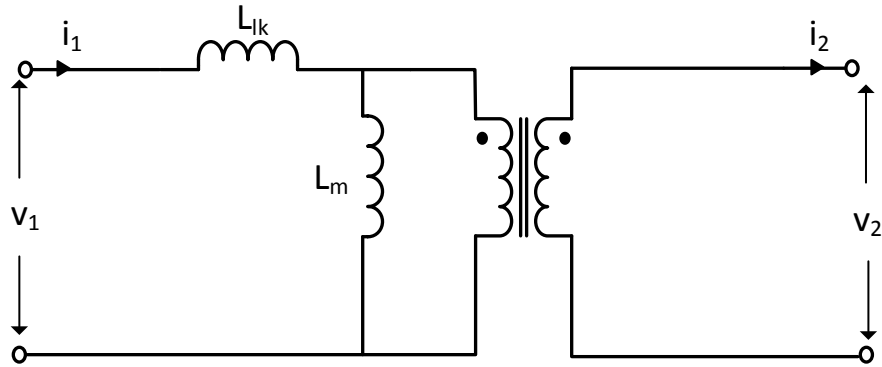


Figure 1.18 Equivalent circuit of a transformer referred to primary side

Generally, leakage inductance of transformer is considered as parasitic and design is optimized to reduce it as much as possible. This leakage inductance causes unnecessary spikes in converter due to its stored energy. But in LLC converter, this parasitic inductor can be put to effective use. As discussed in Section 1.3.4 this inductor is responsible for resonant frequency. The accurate value of the inductor is necessary which has to be ensured in the design of

transformer. Some of the issues with this design are it is difficult to tightly control the leakage inductance of transformer and the secondary side leakage inductance causes voltage stress on the rectifier diode which requires the diode with higher voltage rating.

The major issue of tight control over leakage inductance can be addressed with integrated planar magnetic design of transformer. As discussed in section 1.1.1, the planar technology provides precise control over magnetic parameters and also the repeatability of leakage inductance is ensured which is essential for LLC converter due to vital role of resonant inductor. It also has better reliability. The thesis is focused on design of integrated planar transformer for LLC converter application.

1.5 Thesis organization

In Chapter 1, the planar magnetic technology and LLC converter are reviewed. The requirement of integrated magnetics for LLC converter application is presented.

Chapter 2 deals with the analytical design of transformer with air gap. The design equations for the transformer are provided and design flow is discussed.

Chapter 3 introduces finite element based design of transformer. Based on analytical design results, transformer structure is arrived and simulated in electromagnetic finite element software.

Chapter 4 deals with the optimization of structure of transformer to reduce copper losses in windings. The eddy current effects due to skin effect and proximity effect are introduced and dealt in detail.

Chapter 5 provides details about the design modification to achieve required leakage inductance of transformer. A magnetic shunt is introduced as another layer in the transformer to improve the leakage inductance.

Chapter 6 provides summary and conclusion of the design of integrated transformer and outline for future works.

CHAPTER 2

DESIGN EQUATIONS OF TRANSFORMER

2.1 Introduction

As the magnetic requirement varies based on the specifications of application, it is typically impossible to use off shelf component. For an LLC converter, since there is advantage in designing a transformer with a specific magnetizing and leakage inductance, the transformer design becomes major part of converter design. The design equations and design flow of integrated transformer are discussed in the following section.

2.2 Design equations

The design equations are discussed with the assumption that the LLC converter design is completed and the values for resonant tank are available. From the design specifications, input voltage (V_{in}), Output voltage (V_o) and output current (I_o) are obtained. From the design of LLC Converter, the values for resonant inductance (L_r), magnetizing inductance (L_m), primary current (I_{pri}), secondary current (I_{sec}) peak magnetizing current (I_{mpk}), resonant frequency (f_r), switching frequency (f_s) are obtained. If the magnetizing current and resonant current are not available, they can be calculated from the equations given by equations 2.1 and 2.2. [27]

$$I_{mpk} = \frac{n \cdot V_o}{4 \cdot L_m \cdot f_r} \quad (2.1)$$

$$I_{pri} = \sqrt{\frac{n^2 V_o^2 (2f_r - f_s)}{32 L_m^2 f_r^3} + \frac{\pi^2 I_o^2 f_r^2}{8 n^2 f_s^2}} \quad (2.2)$$

where n is turns ratio.

The turns ratio is generally decided during the design of converter itself. It is given by

$$n = \frac{V_{in}}{V_0} \text{ for full bridge.} \quad (2.3)$$

$$n = \frac{V_{in}/2}{V_0} \text{ for half bridge application.} \quad (2.4)$$

V_{in} is nominal input voltage in varying input application.

Let's define some design factors,

1. *Winding utilization factor (k_w):*

It is defined as ratio of total conduction area of conductors (W_{cond}) to the window area of the core (W_a).

$$k_w = \frac{W_{cond}}{W_a} \quad (2.5)$$

It generally varies from 0.2-0.8. In planar transformers, since the winding is made with PCB and usage of insulation layers results in poor utilization. It is typically in the range of 0.2 to 0.4. The window utilization factor for primary winding is given by [22]

$$k_{wpri} = k_w \frac{1}{\left(1 + \frac{2I_{sec}}{n * I_{pri}}\right)} \quad (2.6)$$

2. *Loss factor (K_{loss}):*

To start with the initial design, a loss factor is assumed. This is the factor which relates dc copper loss (P_{dc}) with the total loss. The relation is given below

$$P_{total} = (1 + k_{loss})P_{dc} \quad (2.7)$$

2.2.1 Area product

Area product of the magnetic core is the product of window area of core (W_a) and the cross-sectional area of the core (A_c). The proper magnetic core for the application is selected based on this value. It is given by [22]

$$Ap = \left[\frac{\sqrt{k_w(1+k_{loss})} L_m I_{pri} I_{mpk}}{B_m k_d k_{wpri} \sqrt{\Delta T}} \right]^{\frac{8}{7}} \quad (2.8)$$

where B_m is maximum flux density, k_d is dimensional parameter of the core and its value is 48.2×10^3 which was arrived based on extensive analysis of several core types and sizes [3] and ΔT is rise in temperature allowed for the design.

2.2.2 Determination of airgap

Generally, airgap is provided in inductors to prevent saturation. In high current transformers, due to higher mmf the core typically saturates when there is no air gap. The core with airgap makes inductance less dependent on relative permeability of the core. This makes the inductance of transformer almost constant throughout the load range. It makes the flux density of the core linear as shown in Figure 2.1. The relationship between flux and coercive force (H) becomes linear for large range of H . It also reduces maximum flux in the core which reduces core losses.

There are some disadvantages in adding gap to the core. There will be fringing flux near the air gap as the magnetic field do not have defined path in air. This fringing flux increases eddy current loss in the winding leading to higher copper loss in winding.

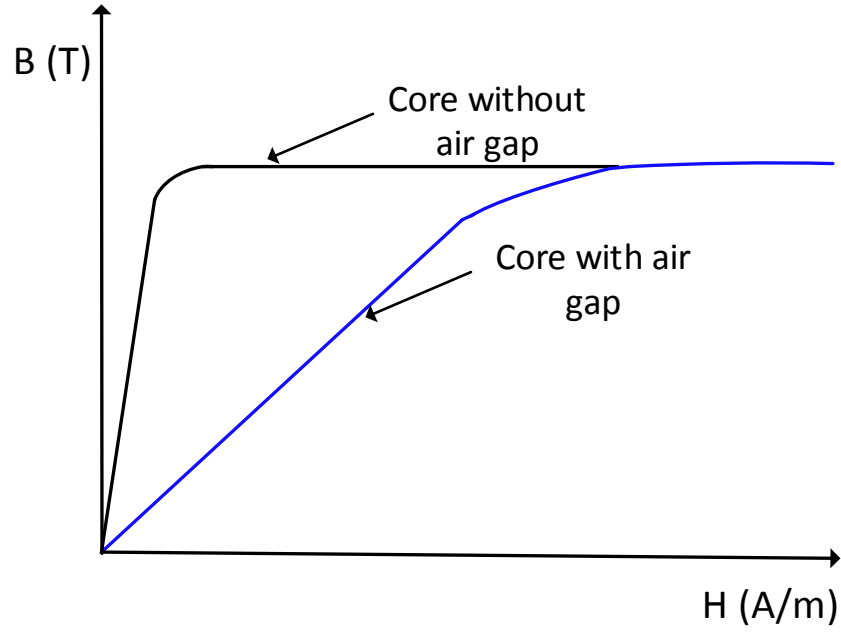


Figure 2.1 B-H curve of magnetic core with and without airgap

Adding a gap to the core modifies the effective permeability of the core assembly. The effective permeability (μ_e) for the core is derived as follows.

Magnetizing Inductance is given by,

$$L_m = \frac{\mu_0 \mu_e N_{pri}^2 A_c}{l_c} \quad (2.9)$$

where N_{pri} is number of primary turns , l_c is the length of magnetic path in core.

Peak Magnetizing current is given by,

$$I_{mpk} = \frac{B_m l_c}{\mu_0 \mu_e N_{pri}} \quad (2.10)$$

From equation 2.9 and 2.10,

$$L_m I_{mpk}^2 = \frac{B_m^2 A_c l_c}{\mu_0 \mu_e} \quad (2.11)$$

On rearranging equation 2.11,

$$\mu_e = \frac{B_m^2 A_c l_c}{\mu_0 L_m I_{mpk}^2} \quad (2.12)$$

As we have selected the core, we can obtain the values for l_c and A_c from the core datasheet. From the effective permeability, the airgap value can be calculated.

The airgap can be placed in center limb of core or it can be evenly distributed in all three legs of core. Gap in outer legs may lead to electromagnetic interference due to fringing flux. Gap in center leg ensures the leakage flux is confined within the transformer. So airgap in center limb is preferred. To find the airgap, let's take a simple core as shown in Figure 2.2. It is magnetically equivalent to a core with an air gap and mmf source in center limb. The length of magnetic path in core is l_c without air gap and a gap of length l_g is introduced in the core. The reluctance of the core with air gap is sum of the reluctances of core and air gap. This can be established as equation 2.13 where A_c is cross sectional area of the core.

$$\frac{l_c}{\mu_0 \mu_e A_c} = \frac{l_c - l_g}{\mu_0 \mu_e A_c} + \frac{l_g}{\mu_0 A_c} \quad (2.13)$$

On simplifying the above equation for l_g , the relationship between l_g , l_c and μ_{eff} is given by equation 2.14.

$$l_g = l_c \left[\frac{1}{\mu_e} - \frac{1}{\mu_r} \right] \quad (2.14)$$

2.2.3 Thermal considerations

The heat generated by the core and copper losses of transformer has to be dissipated through its surface. The proper thermal design is necessary to ensure the temperature does not rise

significantly. The ferrite cores used in the transformer has low Curie temperature. Typically the manufacturer specifies the operating range and from the converter design we get to know allowable maximum temperature. With these data in hand, the losses and other design factors has to be appropriately selected to limit the operating temperature of transformer.

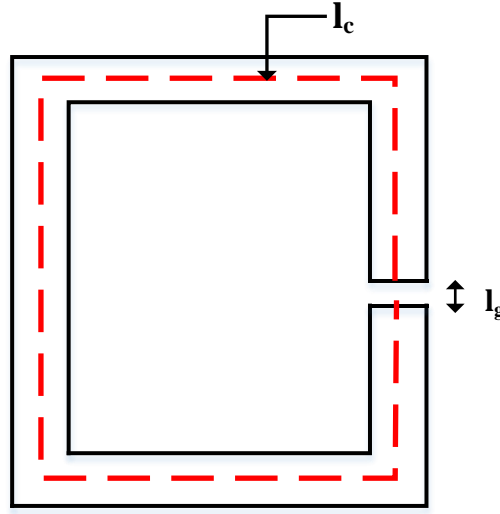


Figure 2.2 Simple core with an airgap

The typical cooling mechanism adopted for transformer in most of the design is convection.

The basic relationship for convective heat transfer is

$$Q = hA_s(T_r - T_a) \quad (2.15)$$

In the equation 2.15, Q represents total power loss in transformer, h is heat transfer co-efficient, A_s is surface area of core, T_r is maximum temperature allowed and T_a is the ambient temperature.

Equation 2.15 can also be represented as

$$\Delta T = R_{therm} Q \quad (2.16)$$

where $\Delta T = T_r - T_a$, rise in temperature and R_{therm} is thermal resistance

R_{therm} is equal to inverse of product of heat co-efficient and surface area (hA_s). Typically for convection through ambient air, $h = 10 \text{ W/m}^2 \text{ }^\circ\text{C}$. The manufacturers may provide the thermal resistance for cores. It can also be calculated from the volume of core (V_c) [3] as

$$R_{therm} = \frac{\sqrt{0.06}}{V_c} \quad (2.17)$$

From equation 2.16, maximum loss allowed for given temperature rise can be calculated.

2.2.4 Determinations of winding parameters

The core manufacturer typically provides A_L value of core in nH/square turn for various air gap lengths of core. A_L value is the inductance factor and it is related to inductance by

$$A_L = \frac{L}{N^2} \quad (2.18)$$

where L is the inductance of the core for N number of turns.

If A_L is not provided then it can be calculated from the equation 2.19 which is obtained from 2.9,

$$A_L = \frac{\mu_0 \mu_e A_c}{l_c} \quad (2.19)$$

If A_L value for the calculated air gap is not available then some other core with closer A_p value and effective permeability value can also be selected. From A_L , the number of turns for primary winding can be calculated from equation 2.20.

$$N_{pri} = \sqrt{\frac{L_m}{A_L}} \quad (2.20)$$

The number of secondary turns can be calculated from the turn ratio,

$$N_{sec} = \frac{N_p}{n} \quad (2.21)$$

To determine conductor dimension, the current density in winding has to be calculated.

It is given by

$$J = k_d \sqrt{\frac{\Delta T}{k_w(1+k_{loss})}} \frac{1}{\sqrt[8]{A_p}} \quad (2.22)$$

We know the conductor area can be related to current density and current as

$$A_{cond} = \frac{J}{I_{pri}} \quad (2.23)$$

The skin depth (δ) determines the thickness of the conductor,

$$\delta = \sqrt{\frac{\rho}{\pi * f_s * \mu}} \quad (2.24.1)$$

where ρ is resistivity of copper.

For copper conductor, by substituting constants, equation 2.24.1 can be simplified as,

$$\delta = \frac{65.2}{\sqrt{f_s}} \text{ mm} \quad (2.25.2)$$

Generally, conductors used for planar transformer has rectangular cross section both in PCB and flat copper winding. The following condition must be satisfied [18] for a typical rectangular cross section shown in Figure 2.3 carrying high frequency current.

$$t \ll w$$

$$t \ll \delta$$

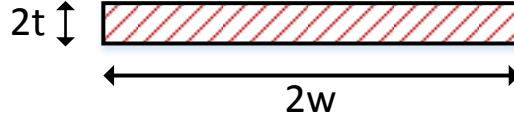


Figure 2.3 conductor with rectangular cross section

Appropriate thickness must be based on the above condition. The width of the conductor can be calculated after selecting thickness.

2.3 Loss calculation

Any magnetic component has two types of losses, one is core loss and other is conduction loss or copper loss. The high frequency magnetic component experiences eddy currents in conductor which leads to increase in copper losses. The analytical calculation of core loss and high frequency copper loss are discussed in this section.

2.3.1 Core loss calculation

The magnetic core experiences alternating magnetic field. This varying magnetic field results in hysteresis loss and eddy current loss. The contribution of hysteresis loss to total loss is significant at low frequencies whereas eddy current losses are significant at higher frequencies [19]. It can be obtained from Steinmetz equation

$$P_c = V_c C_m f_s^x B_m^y \quad (2.26)$$

where V_c is volume of the core, the values of parameters C_m, x, y are generally given by core manufacturer or it can be obtained loss data curve of the core material.

2.3.2 High frequency eddy current loss calculation

The transformer in the LLC converter carries high frequency current which produces high frequency loss due to skin effect and proximity effect. The increase in resistance of the winding due to these effects are called as ac resistance. The ac resistance of the winding is given by well-known Dowell's formula,

$$R_{ac} = R_{dc} * \Delta \left[\varepsilon_1 + \frac{2(p^2 - 1)}{3} \varepsilon_2 \right] \quad (2.27)$$

$$\text{where } \Delta = \frac{t}{\delta}$$

$$\varepsilon_1 = \frac{\sinh 2\Delta + \sin 2\Delta}{\cosh 2\Delta - \cos 2\Delta}$$

$$\varepsilon_2 = \frac{\sinh \Delta - \sin \Delta}{\cosh \Delta + \cos \Delta}$$

p is number of layers in winding, t is thickness of conductor and δ is skin depth at the switching frequency.

In equation 2.27, the first term ε_1 is associated with the skin effect and second term is associated with the proximity effect. It can be seen that the proximity effect not only depends on skin effect but also number of layers which means arrangement of conductors have significant effect on loss due to proximity effect. This high frequency loss is difficult to calculate accurately and it varies based on winding arrangement. This is dealt in detail in chapter 4.

There will be extra loss due to fringing fields near air gap. The fringing flux causes eddy current losses which cannot be calculated analytically.

2.4 Calculation of leakage inductance

Leakage inductance is associated with the energy stored in the magnetic field of the transformer. For a planar transformer given in Figure 2.4, the leakage inductance is given by [3],

$$L_{lk} = \frac{\mu_0 N_{pri}^2 M L T b}{3w} \quad (2.28)$$

The values b and w are breadth and width of winding which can be determined only after winding design. This indicates leakage inductance can be calculated only after designing structure of winding.

CHAPTER 3

DESIGN OF INTEGRATED PLANAR TRANSFORMER

3.1 Design specification

The design specifications for the planar transformer rated at 3.5kW for a LLC converter application is given in Table 3.1. The transformer is used primarily for galvanic isolation in this application. It has turns ratio of 1:1.

Table 3.1 Design specifications for the integrated transformer

Description of parameter	Symbol	Value
Output Power	P_o	3.5 kW
Output voltage	V_o	400V, 240 V
Switching frequency	f_s	90 kHz, 154 kHz
Turns ratio	n	1
Magnetizing Inductance	L_m	100 μ H
Leakage Inductance	L_r	22 μ H
Ambient temperature	T_a	25 °C
Maximum temperature	T_{max}	100 °C
Primary current	I_{pri}	17.7A

The other required specifications, peak magnetizing current can be calculated from equation 2.1 and secondary current can be obtained from relation between resonant current, magnetizing current and primary current.

3.2 Design results:

A planar transformer is designed for the given specifications based on the design equations discussed in Chapter 2. The design process is explained in this section.

1. *Material Selection:*

Material selected for this design is N95 grade Mn-Zn ferrite. It has saturation flux density of 0.4T at 100 °C. The maximum flux density for the design is selected as 0.1T at 154 kHz and 0.16T at 90 kHz.

2. *Design factors selection:*

The winding utilization factor (k_w) and loss factor (k_{loss}) defined by equation 2.6 and 2.8 respectively. Loss factor is taken as 2 for the design. It means that the total loss will be thrice the dc power loss. The winding utilization factor for the initial design is selected as 0.3.

3. The area product of core is calculated from equation 2.8. The temperature rise is 75 °C which can be observed from specification. The calculated A_p value is $6E^{-8} \text{ m}^2$.
4. Based on the area product, magnetic core is selected. The geometrical parameters of selected core are given in Table 3.2. It is an ER core. Its advantage is reduced winding length due to the cylindrical central limb.
5. From the equation 2.12, with the help of core parameters, effective permeability of the core is calculated. It is calculated as 105. The air gap value for the center limb of the core is calculated as 0.9mm.
6. The A_L value obtained is 280 nH/ T^2 . The core was available with A_L value of 250 nH/ T^2 at airgap value of 1.25mm. The number of turns for primary winding can be calculated from the A_L value.

Table 3.2 Geometrical parameters of the selected ER core

Description of parameter	Symbol	Value
Area product	A_p	60430.23 mm^3
Area of cross-section	A_c	206.2 mm^2
Core magnetic path length	l_c	97.2 mm
Mean length of a turn	MLT	93.93 mm
Window Area	W_a	293.2 mm^2

7. The number of turns of primary and secondary winding are calculated as 20.
8. From the current density of the winding, conductor width is calculated as 9mm and thickness is 0.28mm. The thickness should be less than twice skin depth for a conductor with rectangular cross section and skin depth value at 154 kHz is 0.17mm. The dc resistance of winding calculated is 11.7m Ω .
9. From the above step, winding structure of transformer is designed. Since there are more number of turns, the winding structure was designed with 4 layers with 2.5 turns per layer. The thickness of conductor is also considerably high which necessitates paralleling of winding structure. The designed winding structure is shown in Fig.3.1
10. The dc resistance of each winding is calculated from the structure as 14m Ω . The increase in resistance due to the high frequency effect is calculated from equation 2.24 as 147m Ω .
11. The core loss can be estimated from equation 2.26. The loss parameters are extracted based on curve fitting from the loss data curve given in Fig 3.2

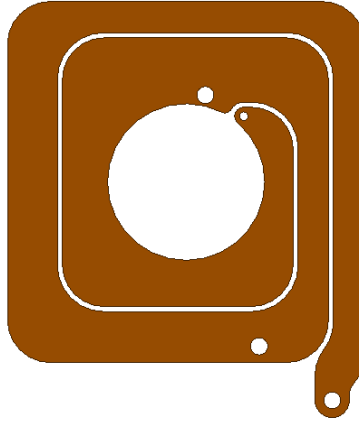


Figure 3.1 Planar PCB winding

The obtained parameters are $C_m = 0.000976$, $x = 2.014$, $y = 2.416$. The flux density in the core is not the same as the initial assumed flux density. The actual flux density in the core can be obtained from equation 3.1 .

$$B = \frac{\mu_0 \mu_e N_{pri} I_{mpk}}{l_c} \quad (3.1)$$

The actual flux density was calculated as 0.076 T and the core loss was obtained as 1.13 W.

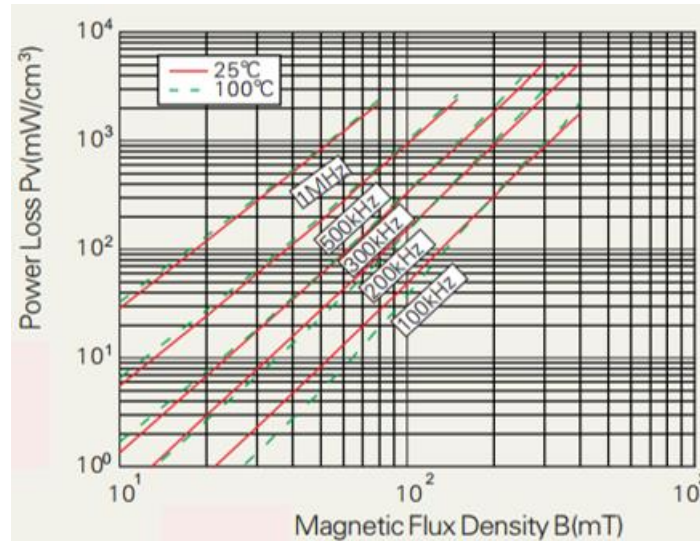


Figure 3.2 Core loss data characteristics curve [28]

12. The structure of designed transformer is shown in Fig.3.3.

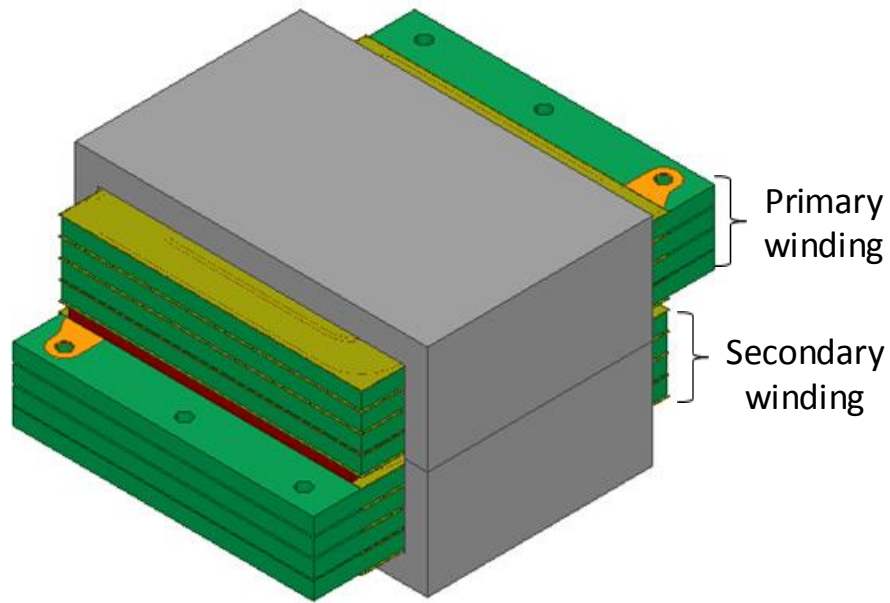


Figure 3.3 Transformer structural arrangement

The 4 winding layers which forms 10 turns are placed in a multilayer FR4 board. There are 4 FR4 boards per winding which gives 20 turns. The structural arrangement is placed in such a way that the each of 2 boards are connected in series and the series connected boards are connected in parallel to each other. Insulation layers which are made of materials like kapton or mylar are placed in between FR4 layers.

The proper structural arrangement of transformer windings define positions of windings in space which would be helpful in determining high frequency losses and leakage inductance. Both high frequency loss and leakage inductance are function of relative position of winding in transformer which are discussed in further chapters.

13. The leakage inductance was calculated based on equation 2.25 and it is obtained as $8.4 \mu\text{H}$.

From the design results, it can be seen that the ac resistance of the winding is significantly

high and the leakage inductance of the transformer has to be improved. The analytical design results are checked with numerical simulations in next section.

3.3 Numerical modeling of transformer:

The employability of analytical method in obtaining solution for complex problem like transformer design has limitations due to non-linearity in characteristics of materials. Leakage inductance and high frequency losses depends on field distribution which cannot be addressed effectively by an analytical method. The analytical solution arrived for transformer design in previous section is verified by numerical solution technique. The Finite element analysis (FEA) is most commonly used computer based numerical modeling technique for electromagnetic structures. In this section, FEA is introduced and its effectiveness in transformer design is discussed.

3.3.1 Electromagnetic finite element analysis:

The finite element method is widely used in engineering problems in many domains like electromagnetics, structural, aerodynamics etc. The numerical methods in electromagnetics computes the distribution of electric and magnetic fields in the structures by solving Maxwell's equation. Any finite element problem not only electromagnetics involves discretization, deriving equations for discretized region and solving the equations [20]. Discretization involves dividing the structure into finite number of elements and closed form solution is obtained for these elements. The advantages of this method are that it can handle nonlinear behavior of structure which cannot be addressed properly by analytical method and good prediction of performance of

structure. But it has disadvantage of high computation time. With the increasing in power of computational systems this is getting reduced drastically since last decade.

Ansys Maxwell software is used for finite element simulations. It supports both magnetic and electric field simulations. There are different types of solvers available in this software. Some of them are electrostatic, magnetostatic, eddy current and transient solvers. The solution type we are interested in, determines the solver. For the high frequency transformer problem, high frequency ac losses are due to flow of eddy currents in windings. This can be obtained with eddy current solver. If we want to estimate parasitic capacitances of transformer, electrostatic solver can be used. As we are interested in estimation of inductance and loss in transformer, eddy current solver is used.

3.3.2 Eddy current solver:

Whenever an alternating current flow through a conductor, time varying magnetic field is produced around the conductor. As per Lenz law, this time varying magnetic field opposes the source of alternating current and generates eddy current resulting in non-uniform current density. It also induces eddy currents in the conductors of its vicinity. This is a frequency domain solver meaning it is based on the assumption that the excitation has single frequency component. The eddy current solver computes eddy current by solving the field equation in (3.2) for vector potential (\mathbf{A}) and electric scalar potential (ϕ).

$$\nabla \times \frac{1}{\mu} (\nabla \times \mathbf{A}) = (\sigma + j\omega\epsilon)(-j\omega\mathbf{A} - \nabla\phi) \quad (3.2)$$

The relationship between vector potential and B field is,

$$\nabla \times \mathbf{A} = \mathbf{B} \quad (3.3)$$

To compute inductance, the average energy is calculated from,

$$W_{av} = \frac{1}{4} \int_V \mathbf{B} \cdot \mathbf{H}^* dV \quad (3.4)$$

where \mathbf{H}^* is complex conjugate of magnetic field \mathbf{H} .

The inductance is then given by,

$$L = \frac{4 * W_{av}}{I_{pk}^2} \quad (3.5)$$

To estimate the ac resistance, the power loss in conductor is calculated from

$$P = \frac{1}{2\sigma} \int_V \mathbf{J} \cdot \mathbf{J}^* dV \quad (3.6)$$

Then the resistance is estimated from the well-known relation between power loss and resistance.

3.3.3 Computation of magnetizing and leakage inductance

The inductance of transformer is computed in eddy current solver as mentioned in Section 3.3.2. The transformer has minimum of two windings one is primary and other is secondary. This results in three inductances which are self-inductances of each winding and a mutual inductance between them. This section deals with obtaining magnetizing and leakage inductances from the inductance matrix comprised of self and mutual inductance. The following notations are used in equations discussed in this section. Subscript 1 indicates the parameter of primary winding and secondary winding parameter is indicated by subscript 2.

The voltage equations of a transformer are given by

$$\begin{aligned} V_1 &= \frac{d\phi_1}{dt} \\ V_2 &= \frac{d\phi_2}{dt} \end{aligned} \quad (3.7)$$

where V_1 and V_2 are voltage at terminals of windings and

ϕ_1, ϕ_2 are flux linkages of the windings.

The flux linkages are related to inductance as,

$$\begin{bmatrix} \phi_1 \\ \phi_2 \end{bmatrix} = \begin{bmatrix} L_{11} & M \\ M & L_{22} \end{bmatrix} \begin{bmatrix} i_1 \\ i_2 \end{bmatrix} \quad (3.8)$$

where L_{11} and L_{22} are self-inductances of winding and M is mutual inductance between windings.

The 4x4 inductance matrix in equation 3.8 is provided by the eddy current solver.

The relation between self-inductance, magnetizing inductance and leakage inductance is

$$\begin{aligned} L_{11} &= L_{lk1} + L_{m1} \\ L_{22} &= L_{lk2} + L_{m2} \end{aligned} \quad (3.9)$$

Here, L_{lk1} and L_{lk2} are leakage inductances of the winding and L_{m1} and L_{m2} are magnetizing inductances of the winding. The magnetizing inductance and mutual inductance are related as

$$L_{m1}L_{m2} = M^2 \quad (3.10)$$

$$\frac{L_{m1}}{L_{m2}} = n^2 \quad (3.11)$$

Here, turns ratio, $n=N_1/N_2$ where N is number of turns

From (3.10) and (3.11), it can be deduced,

$$L_{m1} = n \cdot M$$

$$L_{m2} = \frac{M}{n} \quad (3.12)$$

After computation of magnetizing inductance, leakage inductance can be calculated from the equation 3.9

3.3.4 Simulation results:

The finite element simulation is performed for the transformer structure designed in Section 3.2. The transformer was modeled in 3D and excited with input primary current at operating frequency of 154 kHz. The results are given in Table 3.3 and compared with analytical calculation results.

Table 3.3 Design Result Comparison

Parameters	Spec	Analytical results	Simulation result
Magnetizing Inductance L_m (μ H)	100	100	99.9
Leakage Inductance L_{lk} (μ H)	22	8.4	5.9
Core Loss (W)	-	1.13	1.14
Copper Loss (W)	-	92.1	125.2
Total Loss (W)	< 30	93.25	126.34

From the above results, it can be observed that the leakage inductance and copper loss from analytical calculation and simulation varies significantly. Some of the reason for variation

includes fringing flux at air gap was not considered for analytical calculation. The fringing flux may result in increased eddy currents in conductors. Both the parameters do not meet the specification requirement. Methods to improve the design are discussed in the following chapters.

CHAPTER 4

HIGH FREQUENCY EDDY CURRENT LOSS STUDY

4.1 Introduction

The switching frequencies of the LLC converter are very high due to its reduced switching losses. This makes the magnetic component small but comes with a penalty of increased losses if not designed properly for high frequency. The current in the transformer windings are alternating at high frequency. This high frequency currents generates time varying magnetic field. The eddy currents flow in conductors due to the presence of time varying magnetic field. This results in increased conduction losses known as AC loss. The term AC is used to differentiate increased resistance of winding under AC excitation. The increase in resistance during high frequency operation is due to skin effect and proximity effect. Both the effects cause eddy currents in surface of conductor due to presence of time varying magnetic field which results in non-uniform distribution of current in conductors. This leads to varying current density which increases resistance of conductor. The skin effect and proximity effect are discussed in this chapter and presented methods to diminish these effects.

4.2 Skin effect

As per Lenz's law, time varying magnetic field generated by a current carrying conductor opposes the cause producing it. The cause here is the alternating current flowing in the conductor. The opposition is caused by generating eddy currents in the conductor. This eddy currents tend to flow in a direction to oppose the original AC flux. It results in cancellation of current in center

of round conductor and pushes the current to flow in thin region around the outer surface of the conductor as shown in Fig.4.1.

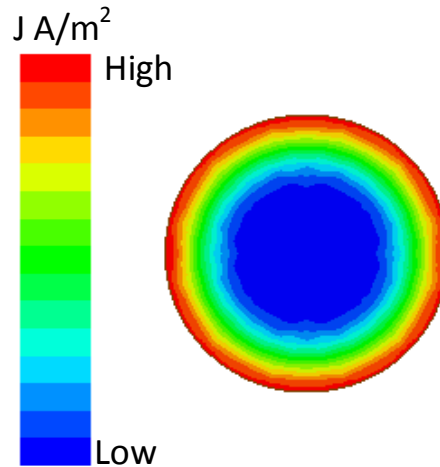


Figure 4.1 skin effect in round conductor

The reduction in current conduction area results in increase of resistance to current flow. This thin region is called as skin depth. This is given by

$$\delta = \sqrt{\frac{\rho}{\pi * f_s * \mu}}$$

It is inversely proportional to square root of frequency of operation. The variation of skin depth with respect to frequency is shown in Fig.4.2. The appropriate conductor dimension should be selected to reduce this effect.

For a rectangular cross section conductor, the current tends to crowd at the edges of the conductor as shown in Fig. 4.3. The skin effect is the behavior of self-inductance of the conductor. It is due to self-induced magnetic field.

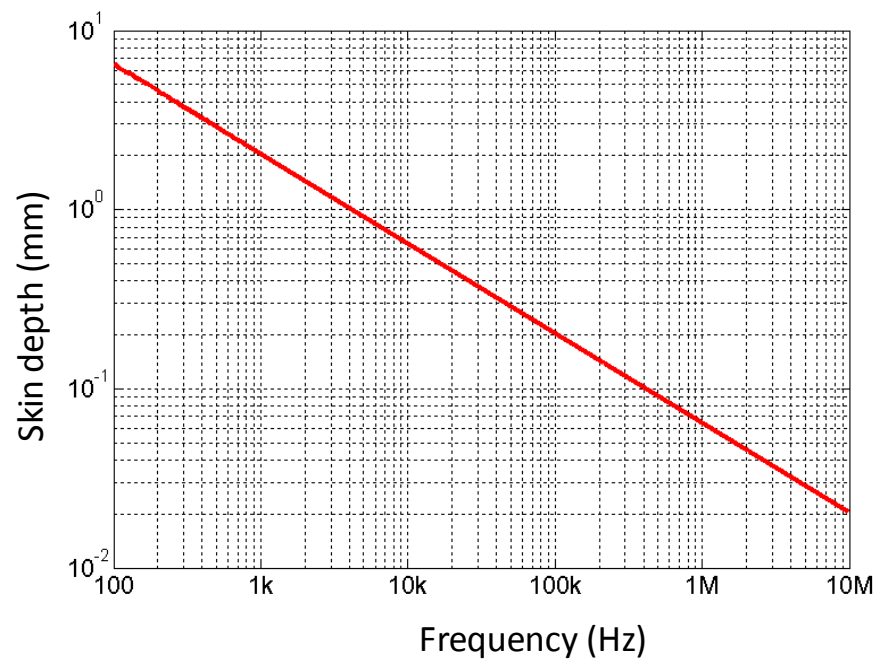


Figure 4.2 Variation of skin depth vs frequency

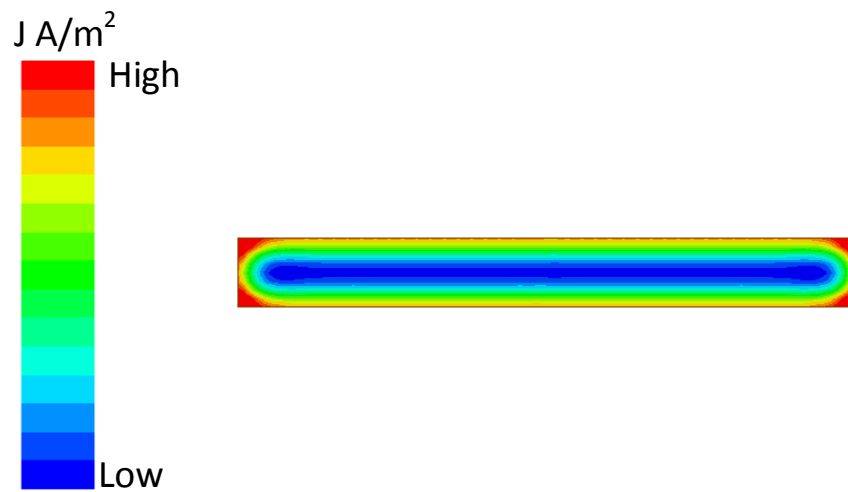


Figure 4.3 skin effect in rectangular section conductor

4.3 Proximity effect

Skin effect is caused by self-induced magnetic field so it takes place in an isolated current carrying conductor in free space whereas proximity effect is caused by coupled magnetic field which occurs when any other conductor are present in vicinity of current carrying conductor . This coupled magnetic field is produced by current carrying conductor in close proximity. It can be said that this effect is a mutual inductance behavior. It interferes with the current in neighboring conductor and causes non-uniform distribution of current in conductor. The proximity effect in a group of conductors is shown in Fig.4.4 for round conductors and in Fig.4.5 for rectangular conductors. All the conductors are carrying current in same direction and current tends to flow away from common center of conductors. This results in increase of resistance leading to higher losses.

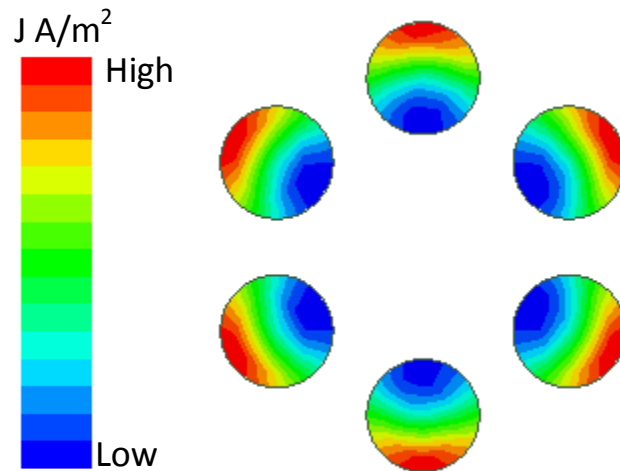


Figure 4.4 Proximity effect in round conductor

Generally, in high frequency magnetics, the loss due to proximity effect is higher than the skin effect. The proximity loss increases with increase in number of layers as mentioned in section 2.3.2. In planar magnetics, tackling proximity effect is not an easy task since most planar

magnetics have multilayer windings due to their reduced winding factor. Next, the physics behind the proximity effect is discussed.

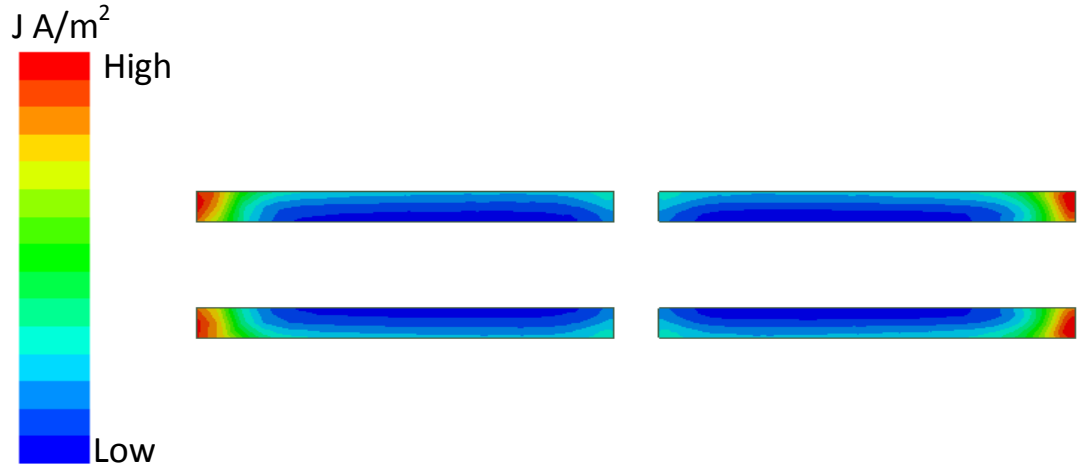


Figure 4.5 Proximity effect in rectangular section conductor

The increase in ac resistance due to high frequency eddy currents was provided by equation 2.24. This is a more simplified form used in analytical calculations. The other form of the Dowell's formula is given by [21]

$$R_{ac} = R_{dc} * \frac{\Delta}{2} [\varepsilon_1 + (2m - 1)^2 \varepsilon_2] \quad (4.1)$$

$$\text{where } \Delta = \frac{t}{\delta}$$

$$\varepsilon_1 = \frac{\sinh \Delta + \sin \Delta}{\cosh \Delta - \cos \Delta}$$

$$\varepsilon_2 = \frac{\sinh \Delta - \sin \Delta}{\cosh \Delta + \cos \Delta}$$

$$m = \frac{F(t)}{F(t) - F(0)}$$

$F(t)$ and $F(0)$ are the magneto motive force (MMF) at the boundary of conductors in transformer. The MMF highly depends on the winding arrangement and their connection in the transformer.

4.3.1 MMF in a current carrying conductor

Consider a conductor carrying current of magnitude I , since it has one turn the maximum mmf is equal to the current. When the thickness of conductor (t), is lesser than the skin depth, the current distribution inside the conductor is uniform which makes the mmf to vary linearly across the conductor as shown in the Fig.4.5 where dx is distance across the conductor. The mmf in a given region is equal to the current enclosed by the region which is

$$F = NI = Hl$$

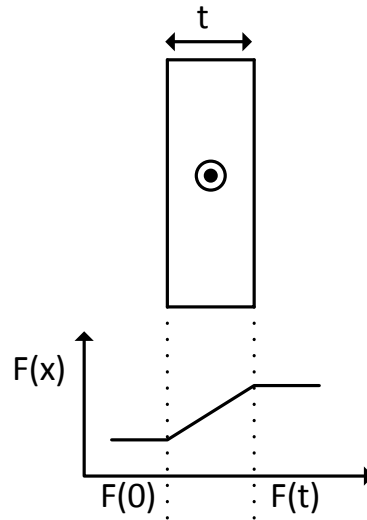


Figure 4.6 MMF across a conductor with uniform current density

4.3.2 MMF in transformer windings

Based on the MMF diagram for a single conductor, MMF diagram is drawn for transformer windings as shown in Fig.4.6. Consider the core of transformer has very high permeability which makes mmf zero in the core. There are three layers of windings both in primary and secondary. Each layer is carrying current of magnitude, i then the total mmf across the primary winding is $3i$ as all the layers are carrying current in same direction which makes the mmf additive. This can be seen in the Fig.4.6. As the secondary winding carries current in opposite direction, mmf starts to reduce on enclosing secondary windings. This MMF diagram is valid when layer thickness is less than the skin depth.

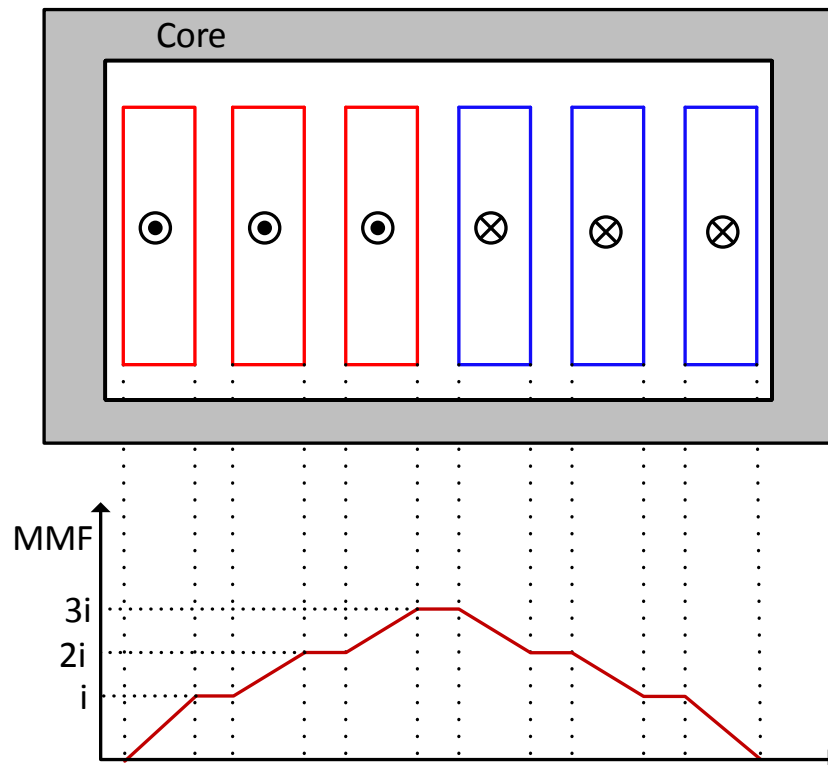


Figure 4.7 MMF in a transformer with multiple layer windings

4.4 Reduction of copper loss due to proximity effect

Based on previous discussion, it can be seen MMF across winding increases when they are additive in nature which happens when winding carrying current in same direction are placed near to each other. If we can reduce the MMF across the winding, then the loss will reduce. To reduce the MMF, the primary and secondary winding layers can be placed beside one another. This concept is called interleaving of windings. The interleaving of windings implemented in our design is discussed in this section.

4.4.1 Interleaved windings

The transformer winding is initially partially interleaved then fully interleaved. The MMF across the windings in all structures are discussed. The MMF across the winding of transformer in non-interleaved condition is shown in Fig.4.6. The MMF is significantly high reaching about 30kA/m which increased the loss significantly.

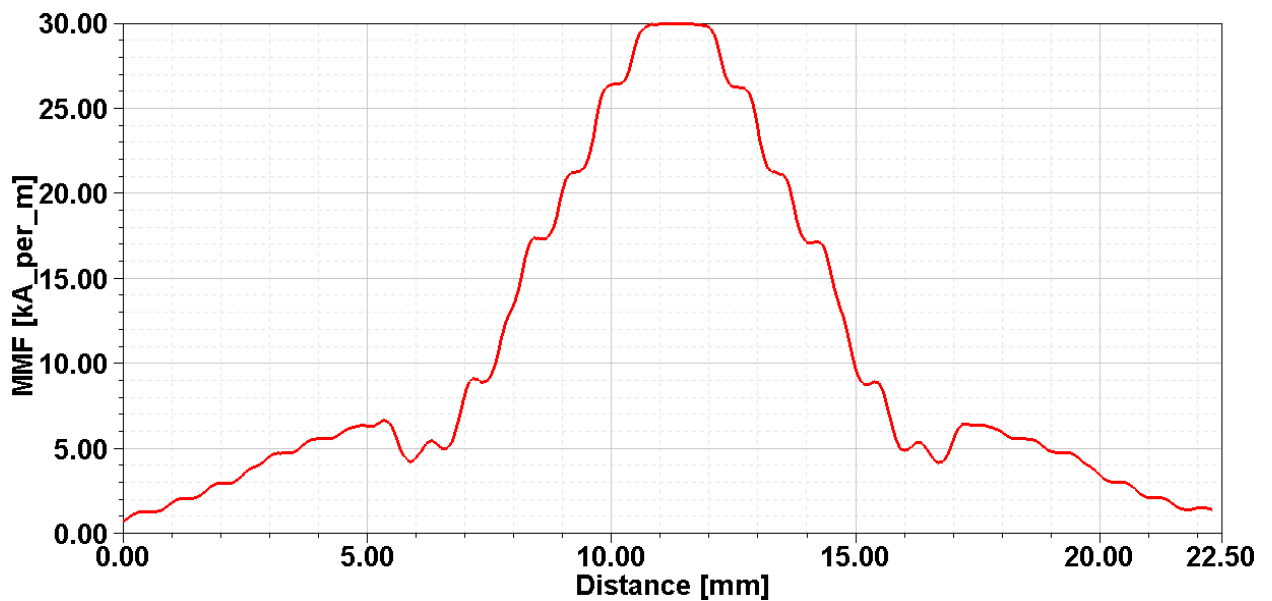


Figure 4.8 MMF in initial design without interleaving

From the MMF plot, it can also be noted that the current is not shared equally among the parallel windings which also contributed to high loss. As mentioned in Section 3.2, there are 4 PCB board per winding, and initially two boards are interleaved meaning 2 boards of primary followed by 2 boards of secondary and so on. The sectional view of structural arrangement of the winding in core is shown in Fig.4.6

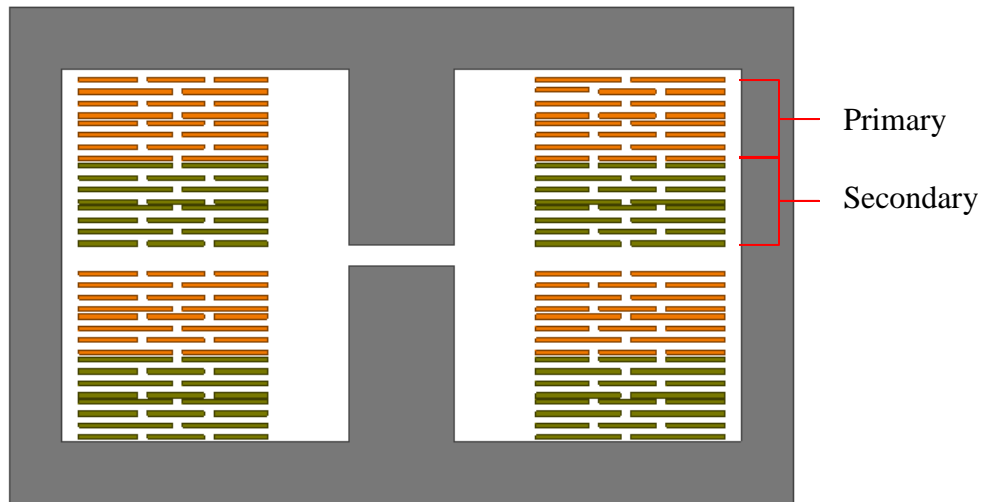


Figure 4.9 Sectional view of partially interleaved structure.

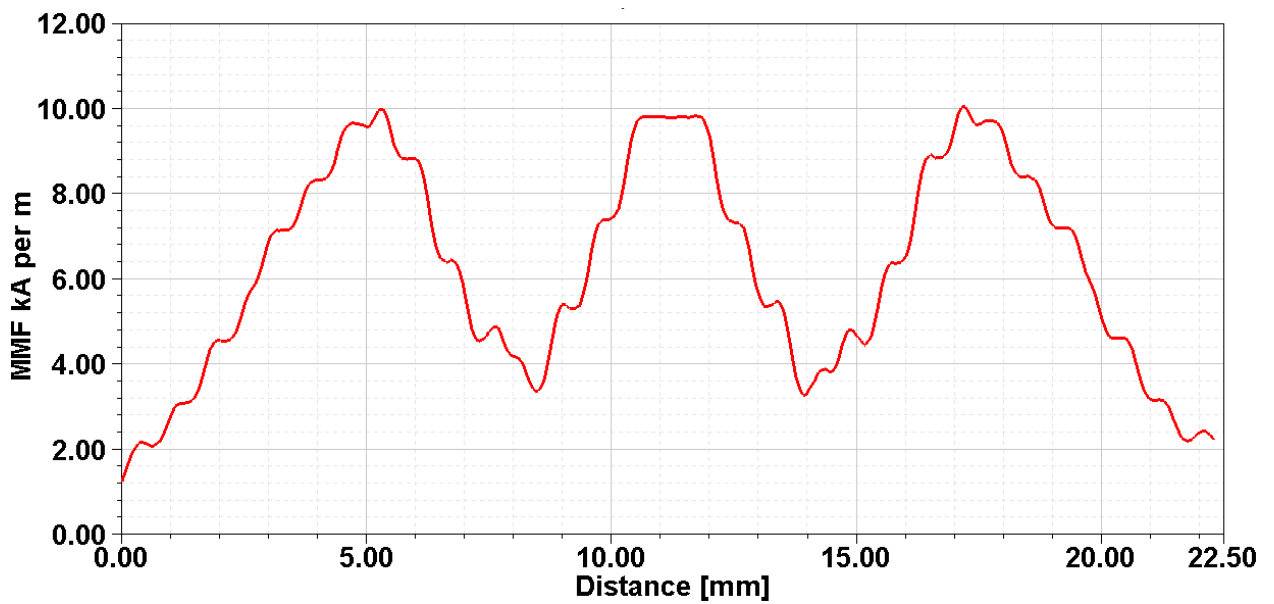


Figure 4.10 MMF in partially interleaved structure

The MMF has reduced significantly to 10 kA/m. It can be observed from the MMF plot, the current is shared equally among all windings. Next, the transformer structure is fully interleaved. The primary and secondary winding PCB's are placed next to each other as shown in Fig.4.9.

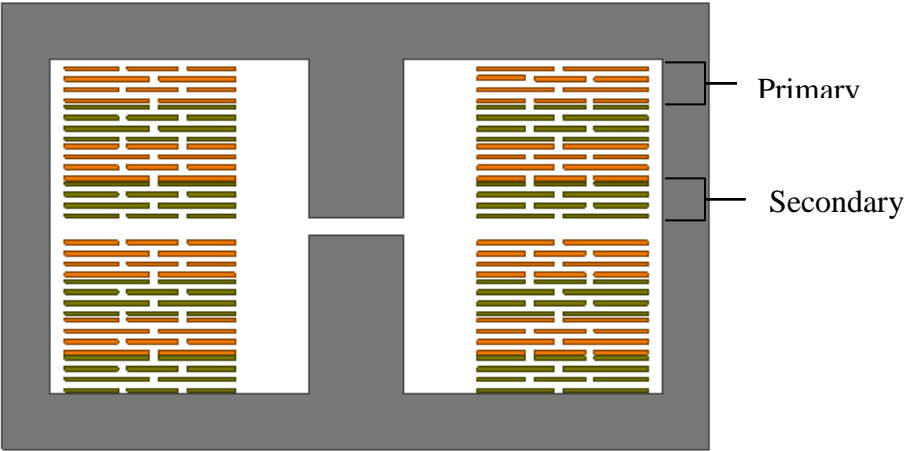


Figure 4.11 Sectional view of fully interleaved structure

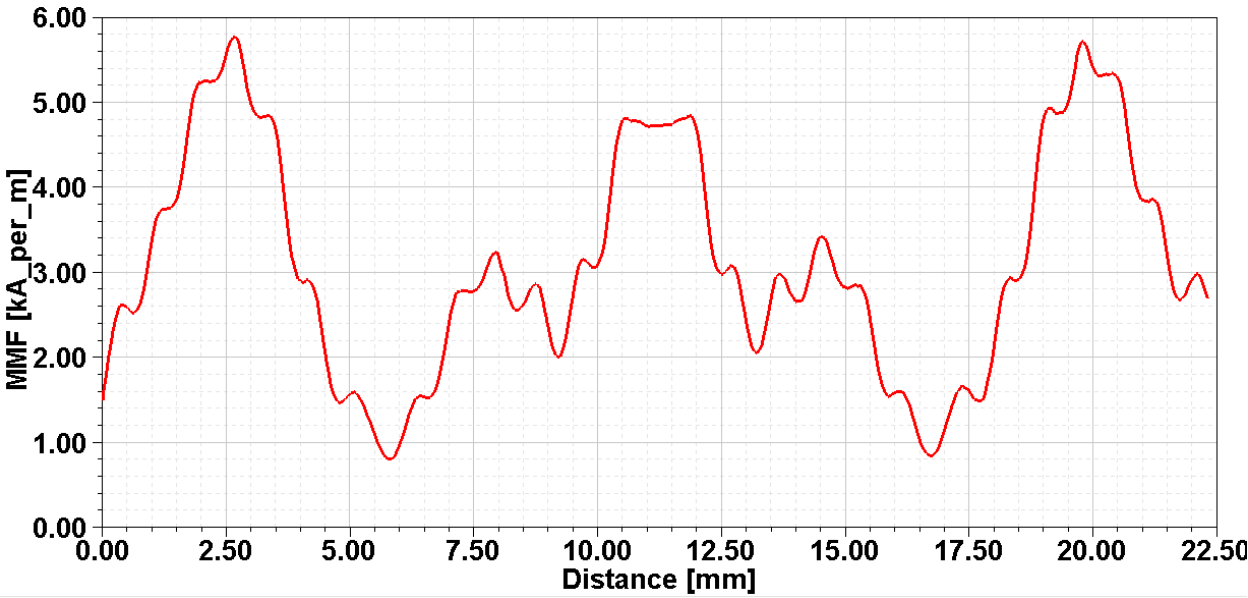


Figure 4.12 MMF in fully interleaved structure

The MMF has reduced much significantly in fully interleaved structure. The simulation results of all the three structures are given in Table 4.1. The copper loss has reduced significantly and it

also comes with disadvantage of reduction of leakage inductance. When the winding MMF reduces, the leakage flux also reduces. This leads to reduction in leakage inductance.

Table 4.1 Simulation results of different winding structures

Parameters	Non -Interleaved	Partially Interleaved	Fully Interleaved
Magnetizing Inductance L_m (μH)	99.9	99.7	99.5
Leakage Inductance L_{lk} (μH)	5.9	2.27	0.67
Core Loss (W)	1.14	1.1	1.02
Copper Loss (W)	125.2	41.4	21.1
Total Loss (W)	126.34	42.5	22.12

4.4.2 Conductor thickness variation study

Conductor thickness was selected as 0.28mm based on the discussion in Section 2.2.4. The selected conductor size is sufficient to overcome skin effect. But due to proximity effect conductor has to be much smaller than the skin depth. A study was performed with varying conductor thickness to check this in 2D simulation. The PCB track thickness was varied from initial design of 8 oz (0.28 mm) to 4 oz (0.14 mm). The change in power loss with the conductor thickness variation is given in Fig.4.9. It can be seen that the loss reduces with reduction in conductor thickness up to 5 oz and increases again. Based on this study, conductor thickness is selected as 5 oz.

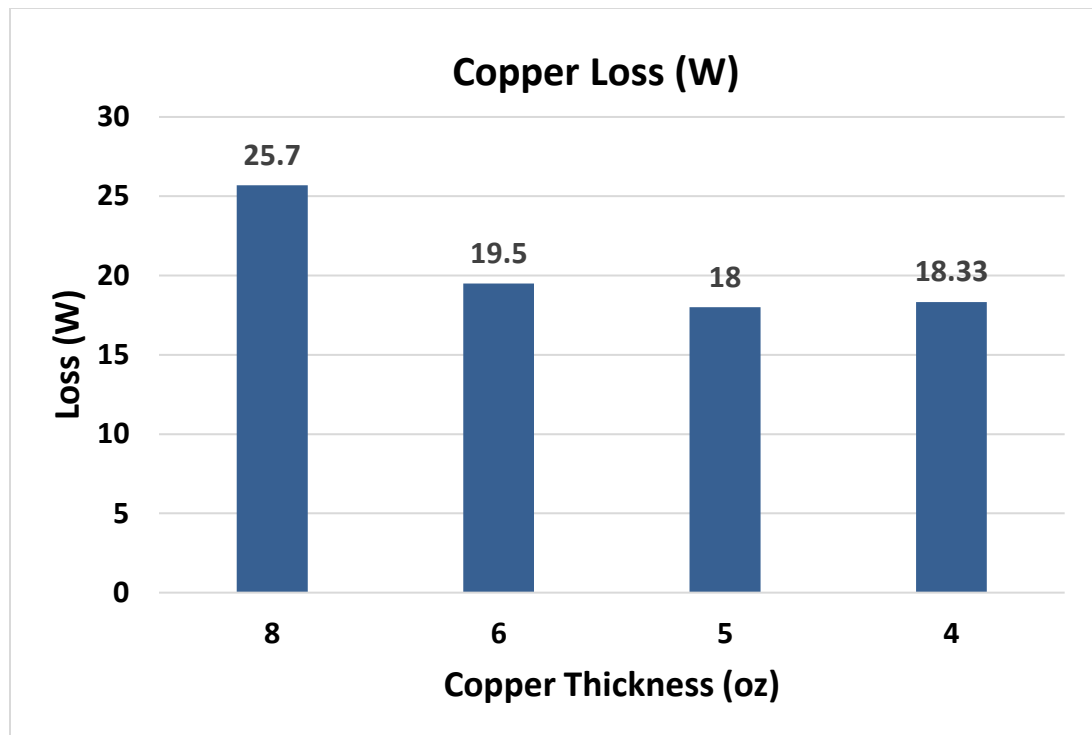


Figure 4.13 Copper loss vs PCB trace thickness

CHAPTER 5

IMPROVEMENT OF LEAKAGE INDUCTANCE

5.1 Introduction

Leakage inductance is the inductance of transformer windings due to the flux which does not flow in its confined path. The flux generated due to the current in windings has to close path only through the magnetic core. But not the complete flux generated flows through the core some will close with winding and core. This flux is called as leakage flux which results in leakage inductance of winding.

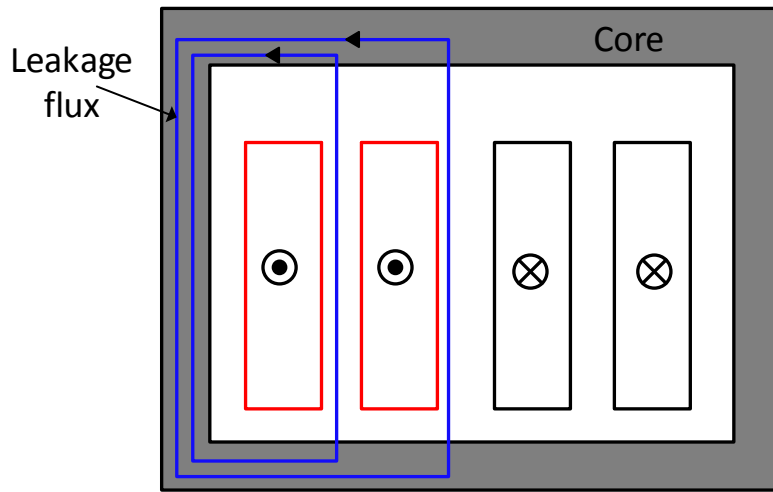


Figure 5.1 Leakage flux

The stored energy in leakage inductance is given by

$$E_{lk} = \frac{1}{2} L_{lk} I^2 \quad (5.1)$$

This leakage inductance can be obtained by short circuiting the secondary winding of transformer and measuring inductance at primary side which gives total leakage inductance. Since the primary

is shorted, the magnetizing flux becomes zero as both primary and secondary carries same current. But the leakage flux flows in the transformer.

5.2 Methods to calculate leakage inductance

There are some methods proposed in literature to calculate leakage inductance [23-26] like stored energy method and reluctance model of transformer method. The calculation of leakage inductance based on stored energy is discussed here and reluctance model is discussed in Section 5.4.

5.2.1 Stored energy method

The leakage inductance is due to the magnetic energy stored in the windings and air region around it. The energy is stored both in primary and secondary windings. The relation between the stored energy and inductance is given by equation 5.1. The energy stored in a magnetic field is given by

$$E_{mag} = \frac{1}{2} \int_V B \cdot H \, dV \quad (5.2)$$

Since energy is stored in air gap between the windings, this equation can be simplified as

$$E_{mag} = \frac{\mu_0}{2} \int_V H^2 \, dV \quad (5.3)$$

From equation 5.3, to calculate the energy we have to obtain the field strength, H which depends on the ampere turns and geometry of the windings. In [23], the H field is assumed to be constant along the plane of the winding layer and upon integration it varies linearly throughout the winding layer instead of becoming constant in between the layers (as in Fig.4.5).

5.3 Methods to improve leakage inductance

Based on the design results in Table 4.1, the leakage inductance has reduced substantially which is clearly evident from equation 5.3. As interleaving the winding, results in reduction of MMF between the layers (shown in Fig 4.6, 4.8 and 4.10) the leakage energy reduces which causes the inductance to decrease. From equation 5.3, the following can be observed to increase leakage inductance,

1. Ampere turns can be increased to increase field strength
2. Geometry of winding and insulation
3. Permeability of material between winding layer

These methods are discussed briefly in this section.

5.3.1 Ampere turn of winding

As the magnetic field strength is proportional to ampere turns, increasing it will increase leakage inductance. Since the current in the transformer is fixed based on the design requirement, number of turns can be increased to increase ampere turns. But it may result in higher copper loss.

If the number of turns has to be increased, the design has to be modified completely since there is no space for extra windings and analytical calculation has to be performed.

5.3.2 Winding and insulation geometry

The stored energy increases with the increase in thickness of copper and insulation layer which can be inferred from equation 5.3. But increasing copper thickness leads to increase in

losses due to skin effect and proximity effect. The insulation layer can be increased to improve leakage inductance but due to high winding factor the design, it is not a feasible solution.

5.3.3 Leakage layer

The permeability of material where energy is stored determines its value as seen in equation 5.3. The permeability of copper, insulation layers play vital role in the energy storage. The permeability can be improved by introducing a material with moderate permeability. Some of the material which are suited well for this are low permeable ferrite materials like Ni-Zn. They act as leakage layer and increases stored energy between the windings to have high leakage flux. This method is a feasible with the current design.

5.4 Design with magnetic leakage layer

A magnetic leakage layer was placed in between the winding layers. The sectional view is shown in Fig.5.2. The magnetic material used is low permeability Ni-Zn ferrite.

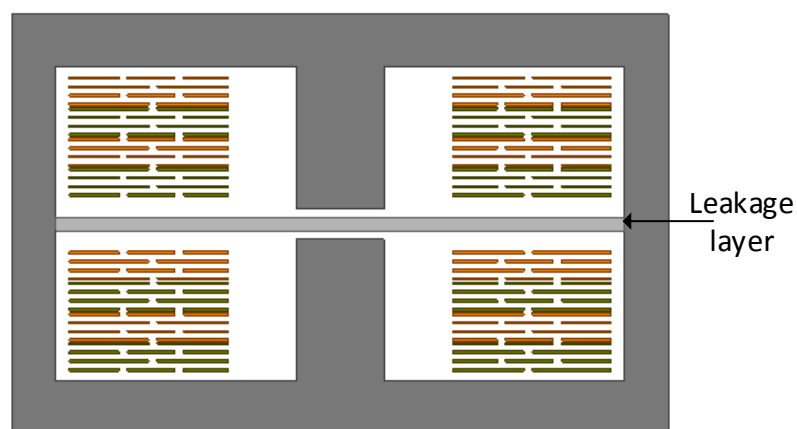


Figure 5.2 Transformer with leakage layer

On placing a magnetic leakage layer, the flux path is modified. The presence of magnetic shunt leads to change in both magnetizing inductance and leakage inductance. So the appropriate magnetic shunt thickness and air gap required has to be determined. In order to find the appropriate magnetic shunt thickness and air gap, both the parameters are varied over certain range.

5.4.1 Magnetic reluctance model of transformer

Due to change in magnetic circuit because of the introduction of magnetic leakage layer, both the magnetizing and leakage inductances varies with airgap, shunt thickness and permeability of the leakage material. In order to understand the relation, a magnetic reluctance model of transformer with magnetic leakage layer was developed. The reluctance model is shown in Fig.5.3. Here, secondary is left open and primary is excited to find magnetizing and leakage inductance.

The magnetizing inductance is given by mutual flux between the windings,

$$L_m = \frac{N_{pri} * \phi_{12}}{I_{pri}} \quad (5.4)$$

The self-inductance and primary winding flux are related as,

$$L_{11} = \frac{N_{pri} * \phi_{11}}{I_{pri}} \quad (5.5)$$

On solving the magnetic circuit in fig.5.3 for primary flux and mutual flux,

$$\phi_{11} = \frac{2N_{pri}I_{pri}(R_{lk}+R_{shw})}{(R_{lk}-2R_{shw})R_{lk}} \quad (5.6)$$

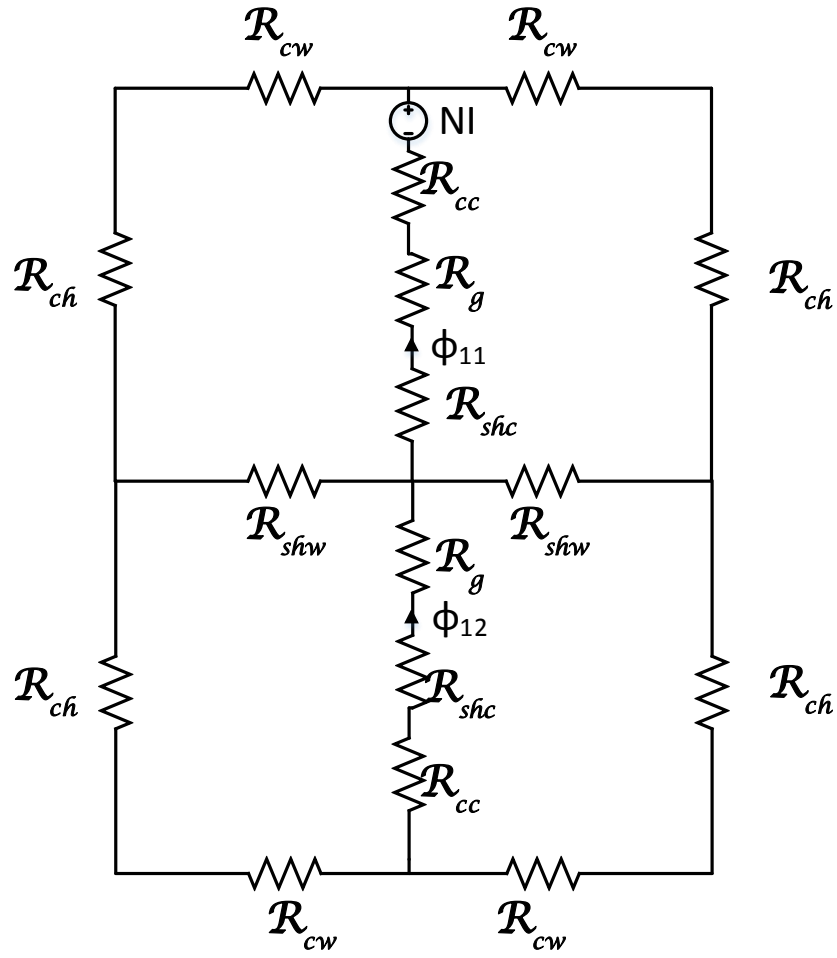


Figure 5.3 Transformer reluctance model

$$\phi_{12} = \frac{2N_{pri}I_{pri}R_{shw}}{(R_{lk}-2R_{shw})R_{lk}} \quad (5.7)$$

where $R_{lk} = R_{cw} + R_{ch} + 2(R_{cc} + R_{shc} + R_g + R_{shw})$.

The primary winding inductance is obtained from equation 5.5 and 5.6 as,

$$L_{11} = \frac{2N_{pri}^2(R_{lk}-R_{shw})}{(R_{lk}-2R_{shw})R_{lk}} \quad (5.8)$$

The magnetizing inductance is obtained from equation 5.4 and 5.7 as,

$$L_m = \frac{2N_{pri}^2 R_{shw}}{(R_{lk} - 2R_{shw})R_{lk}} \quad (5.9)$$

By invoking the relation between leakage inductance and self-inductance given in equation 3.9,

$$L_{lk1} = \frac{2N_{pri}^2}{R_{lk}} \quad (5.10)$$

The reluctance model is applied to the transformer. Since interleaving condition modifies the MMF in the circuit, the non-interleaved design is considered for modeling. The 2D FEA simulations were also performed to check the modeling accuracy. The results of leakage inductance and magnetizing inductance are shown in Fig.5.4 and 5.5 respectively. Magnetic leakage material (Shunt) of permeability 100 is considered for this study.

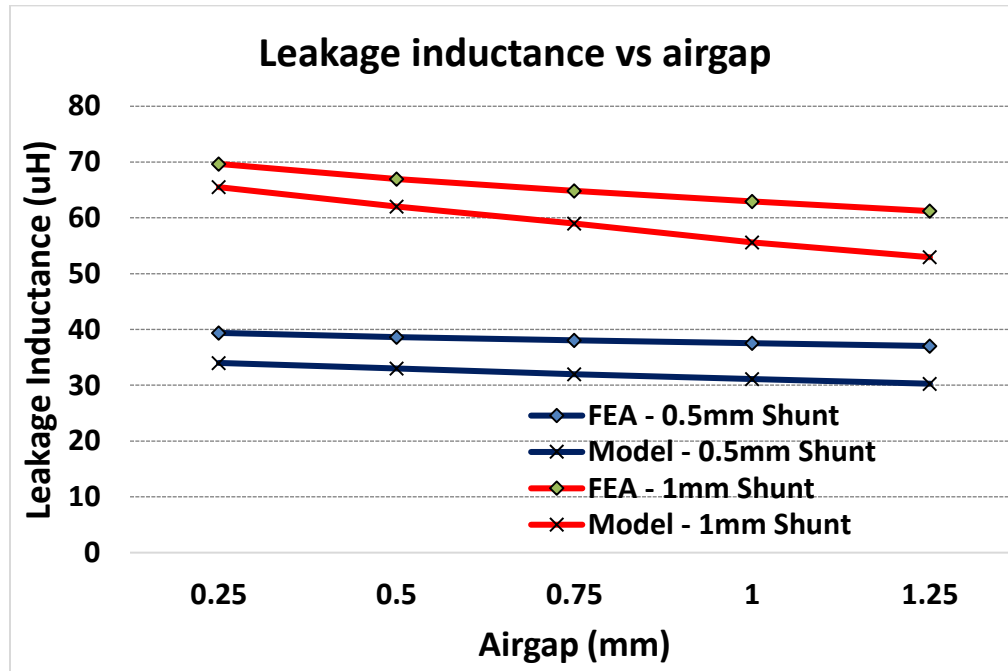


Figure 5.4 Leakage inductance vs airgap length for different shunt thickness

It can be noted in Fig.5.4, the leakage inductance is almost constant at lower air gap length and varies over a small range at higher airgap length. It can be noted that the magnetizing inductance

varies in a narrow range for a given air gap length. The results from model and FEA are close and average variation is about 15%. From this, it can be said the leakage inductance is least dependent on airgap length and mainly varies based on shunt thickness.

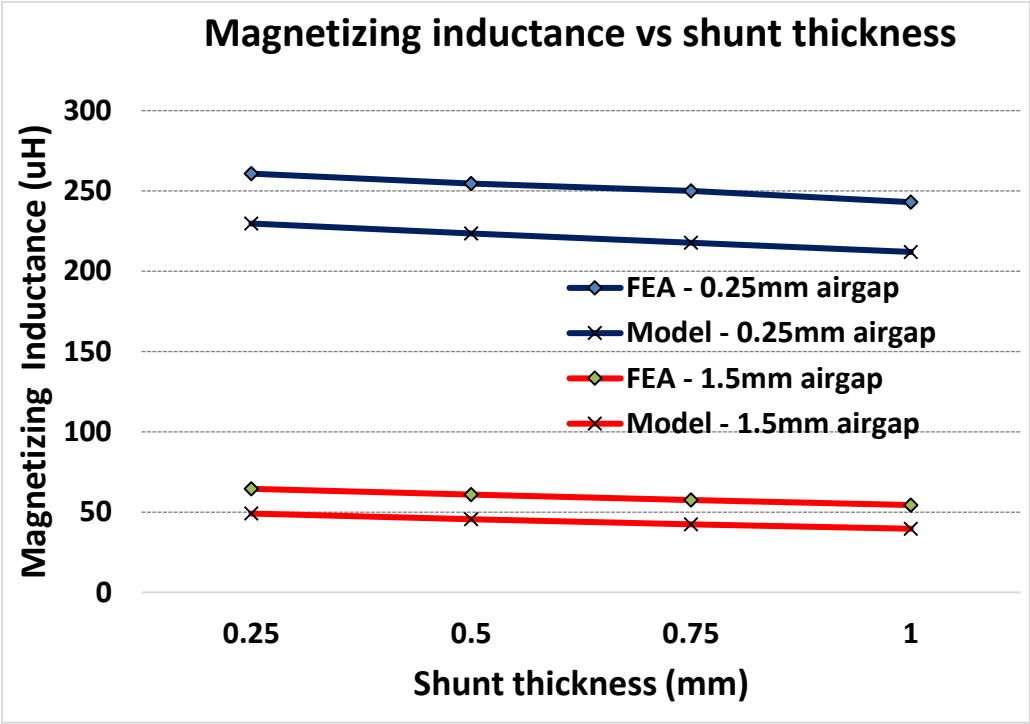


Figure 5.5 Magnetizing inductance vs shunt thickness for different airgap length.

It can be observed in Fig.5.4, the change in magnetizing inductance is less sensitive to magnetic layer thickness and depends heavily on the airgap length. The results from model and FEA are following trend though average variation is about 15 - 25%. From this, it can be said the magnetizing inductance is least dependent on shunt thickness and mainly varies based on airgap length.

The leakage inductance and magnetizing inductance has got decoupled by the introduction of magnetic leakage layer. This gives better advantage as we have independent control over the

inductance values. It can be concluded that the airgap length can be selected based on magnetizing inductance and leakage inductance is selected based on the shunt thickness.

Then the effect of permeability on the inductances are studied. The shunt thickness is fixed as 0.75mm and three permeability values 20, 100 and 200 are taken. The magnetizing inductance and leakage inductance for various airgap lengths are shown in Fig.5.6 and 5.7 respectively. The 2D FEA results are plotted for leakage inductance and not in magnetizing inductance to avoid cluttering of graph.

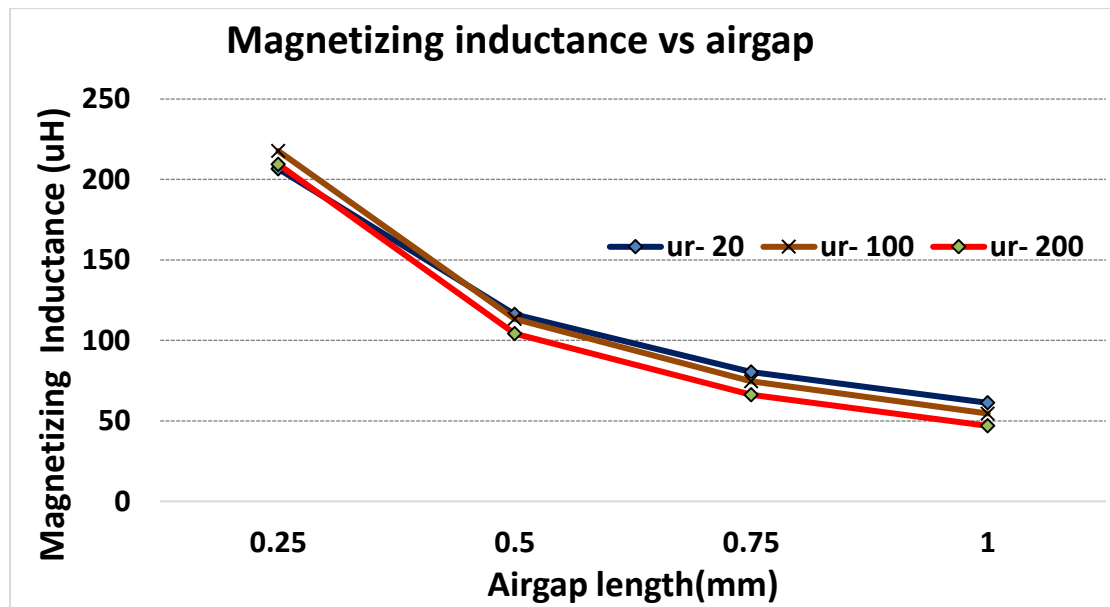


Figure 5.6 Magnetizing inductance vs airgap length for various permeability

The variation in magnetizing inductance for different permeability values is significantly less. As the permeability increases, leakage flux in the structure increases leading to reduced magnetizing inductance which is clearly seen at high airgap lengths. As the permeability of material increases, the variation in leakage inductance over airgap length also increases. This can

be observed in Fig.5.7. All these study are performed in transformer with non-interleaved windings, then the leakage layer is introduced in interleaved design.

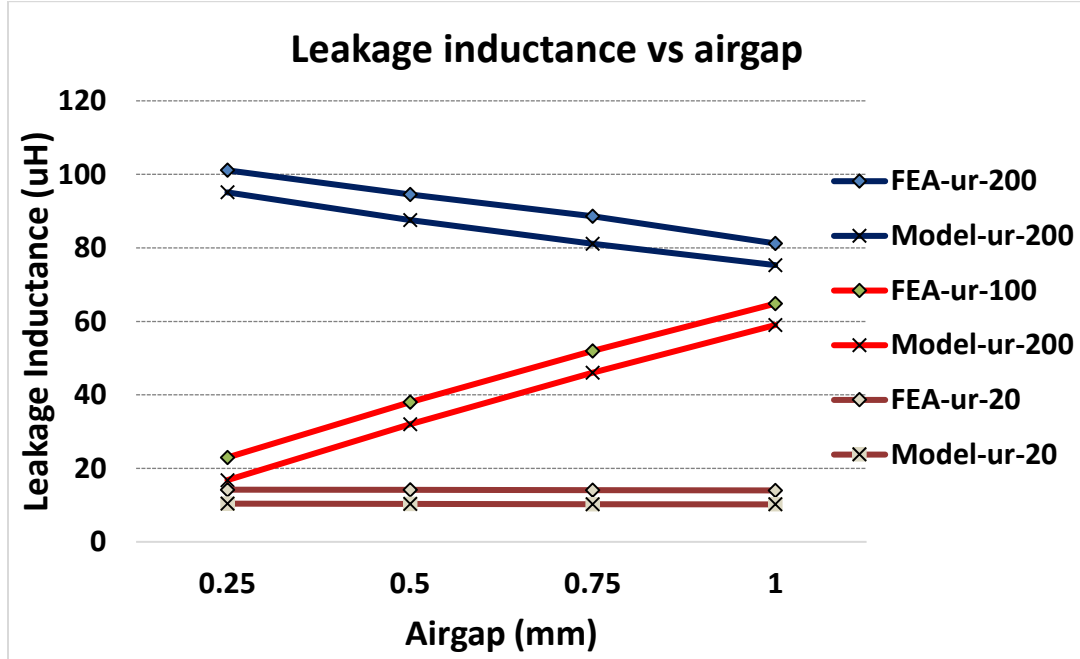


Figure 5.7 Leakage inductance vs airgap length for various permeability values

5.4.2 Leakage layer in fully interleaved winding

Leakage layer of 1mm thickness is introduced in between winding as shown in Fig.5.2 and simulated in 2D FEA. The leakage inductance value obtained was 0.6 μ H. The probable reason could be due to full interleaving, the magnetic field strength between the primary and secondary winding reduces drastically. This results in reduction of leakage inductance.

Partial interleaving could help to increase the leakage inductance but the copper loss will increase. The insulation layer thickness can be increased which may not increase the leakage inductance significantly. The higher ampere turns of the winding necessitates the full interleaving.

If the ampere turns are reduced, it can facilitate partial interleaving which could help to have increased leakage inductance with minimum loss.

5.5 New design with reduced ampere turns

The higher ampere turns was due to high winding factor, the winding factor of this design was reduced to 0.17. The design guidelines followed in section 2.2 is followed and the new design results are shown in Fig.5.8 The selected core parameter is shown in Table 5.1. The core was available with A_L value of 700nH/T^2 and the number of turns is 20.

Table 5.1 Geometrical parameters of the selected EE core

Description of Parameter	Symbol	Value
Area product	A_p	87211.95 mm^3
Area of cross-section	A_c	380.1 mm^2
Core magnetic path length	l_c	96.95 mm
Mean length of a turn	MLT	113.88 mm
Window Area	W_a	229.4 mm^2

The winding is designed as 4 layers with 3 turns per layer. Based on the previous design, the thickness of the conductor was selected as 6oz. The winding has two set of PCB connected in parallel. As the turns got reduced, the proximity effect is also expected to reduce and also since there was significant reduction in copper loss from 8 oz to 6 oz copper thickness, this design was selected to have 6 oz copper.

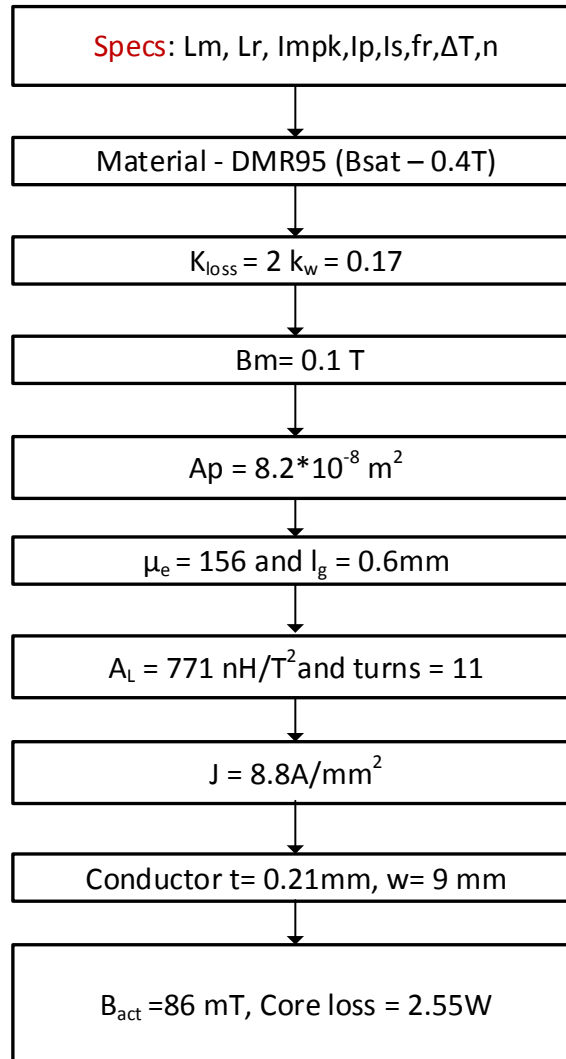


Figure 5.8 New design result

The transformer shown in Fig 5.9 is modelled in 2D FEA and the results are shown in Table 5.2.

The copper loss for various thickness are simulated in 2D FEA which verifies the selection of 6 oz copper, results are shown in Fig.5.11

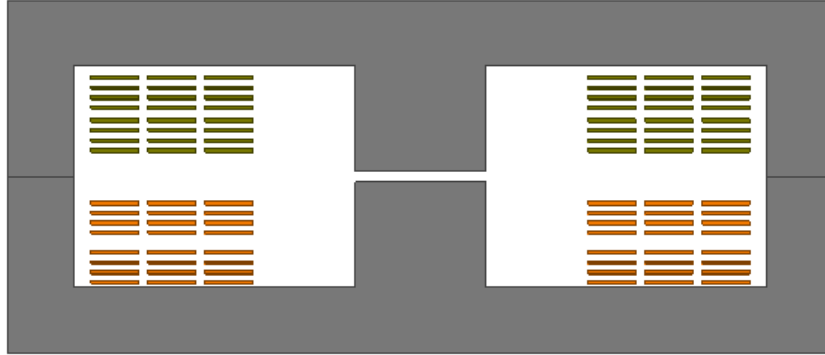


Figure 5.9 2D FEA model

Table 5.2 Design result comparison

Parameters	Spec	Analytical results	Simulation result
Magnetizing Inductance L_m (μH)	100	100.4	100.4
Leakage Inductance L_{lk} (μH)	22	2.44	2.95
Core Loss (W)	-	2.55	1.54
Copper Loss (W)	-	41.2	50.5
Total Loss (W)	< 30	43.75	51.64

The copper loss has greatly reduced compared to previous design. Then the winding is partially interleaved as shown in Fig.5.10. The results of the interleaved design is shown in Table 5.3. The copper loss has reduced substantially to 16.4W. The leakage inductance also has reduced as expected. The leakage layer is introduced to improve leakage inductance and discussed in next section

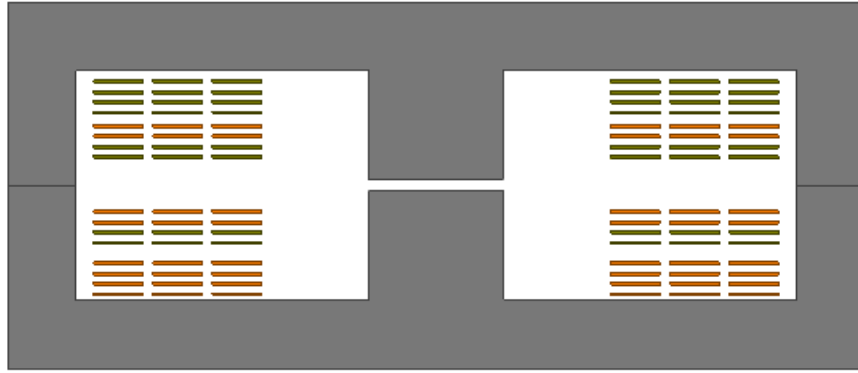


Figure 5.10 Partially interleaved model.

Table 5.3 Partially interleaved winding design result comparison

Parameters	Spec	Non-interleaved winding	Partially Interleaved winding
Magnetizing Inductance L_m (μH)	100	100.4	100.5
Leakage Inductance L_{lk} (μH)	22	2.95	1.1
Core Loss (W)	-	1.54	1.47
Copper Loss (W)	-	50.5	16.4
Total Loss (W)	< 25	51.64	17.87

5.6 Magnetic shunt in new design

Based on the analysis in section 5.4.1, the airgap length with shunt layer is determined since the magnetizing inductance depends mainly on airgap length. The variation in magnetizing inductance for various shunt thickness and airgap is plotted in Fig.5.12. The study is carried out in 2D FEA for magnetic layer permeability of 100,150,200 and 250. From the plots in Fig.5.12,

the airgap length is determined as 0.75mm. The magnetizing inductance remains almost constant for all permeability values.

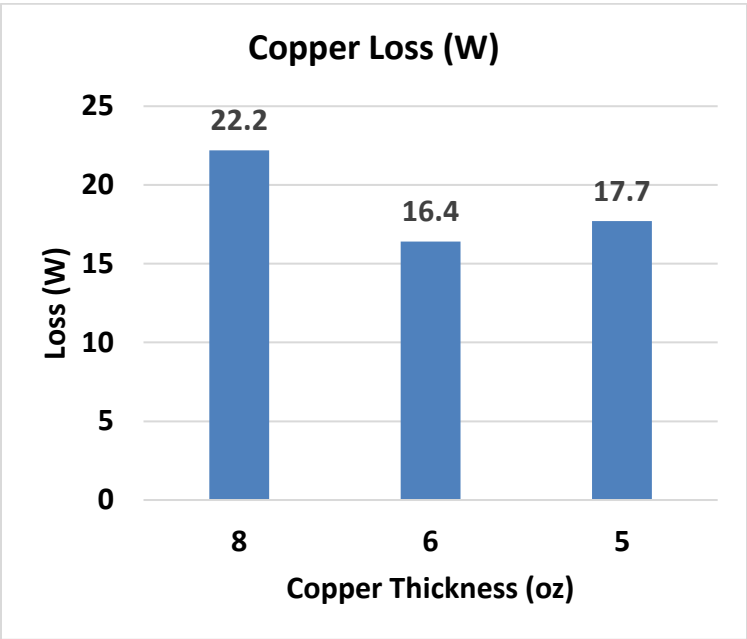
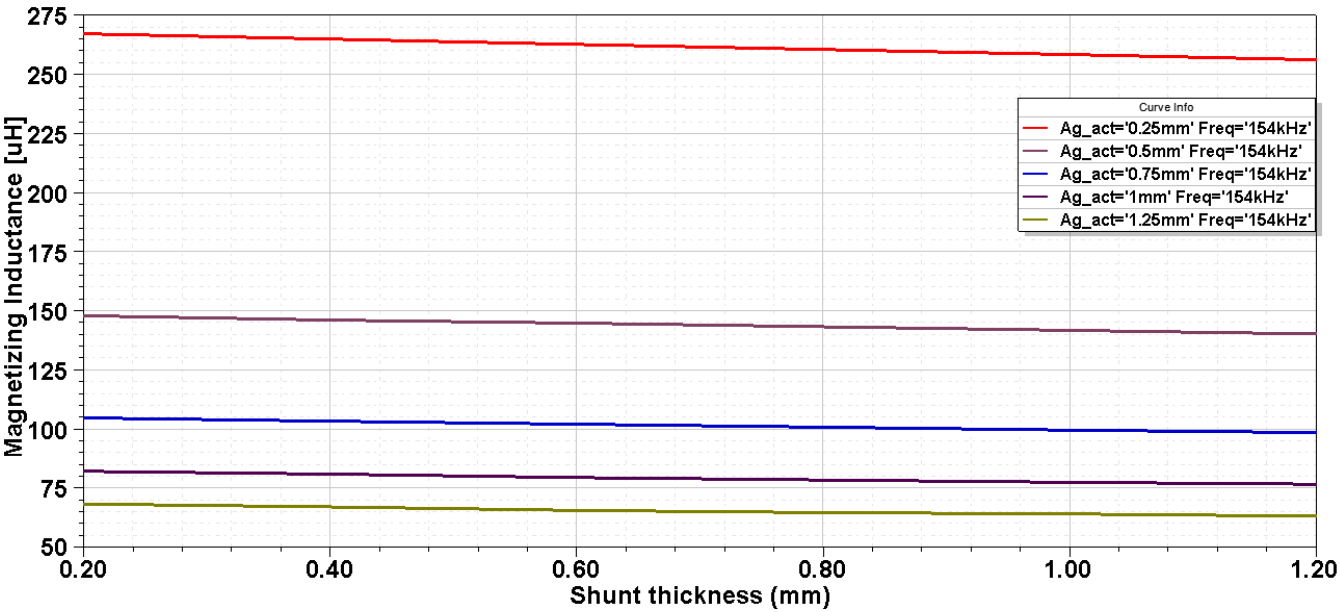
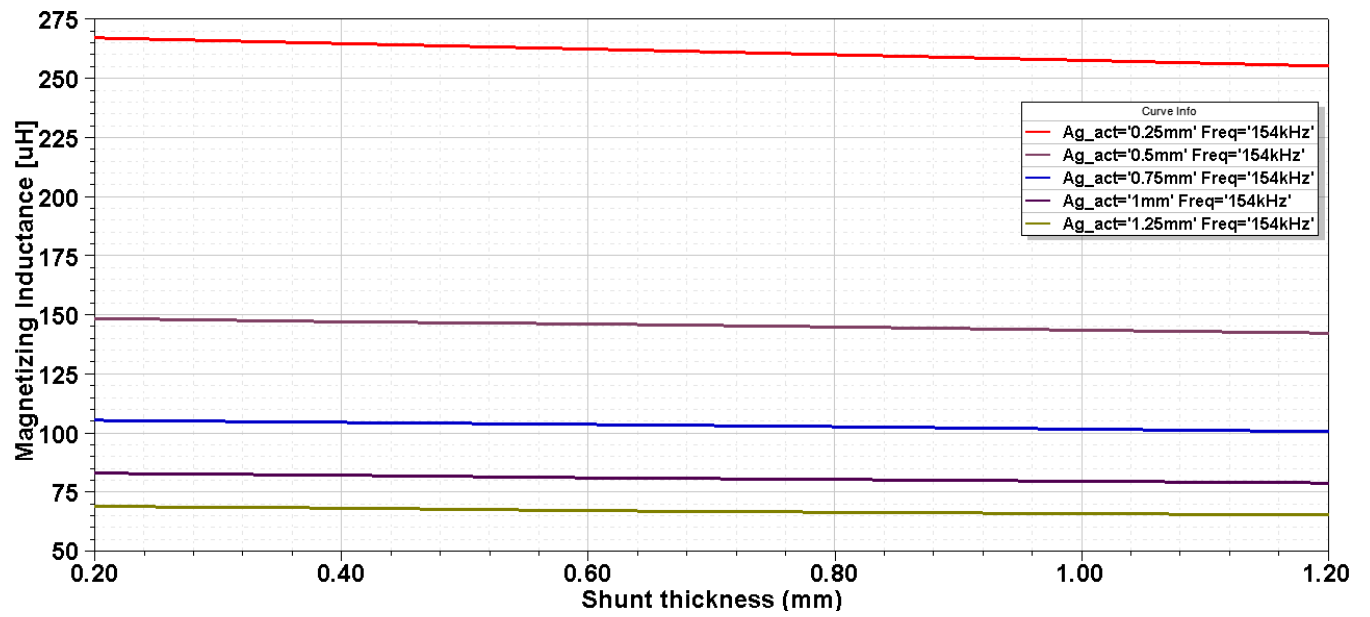


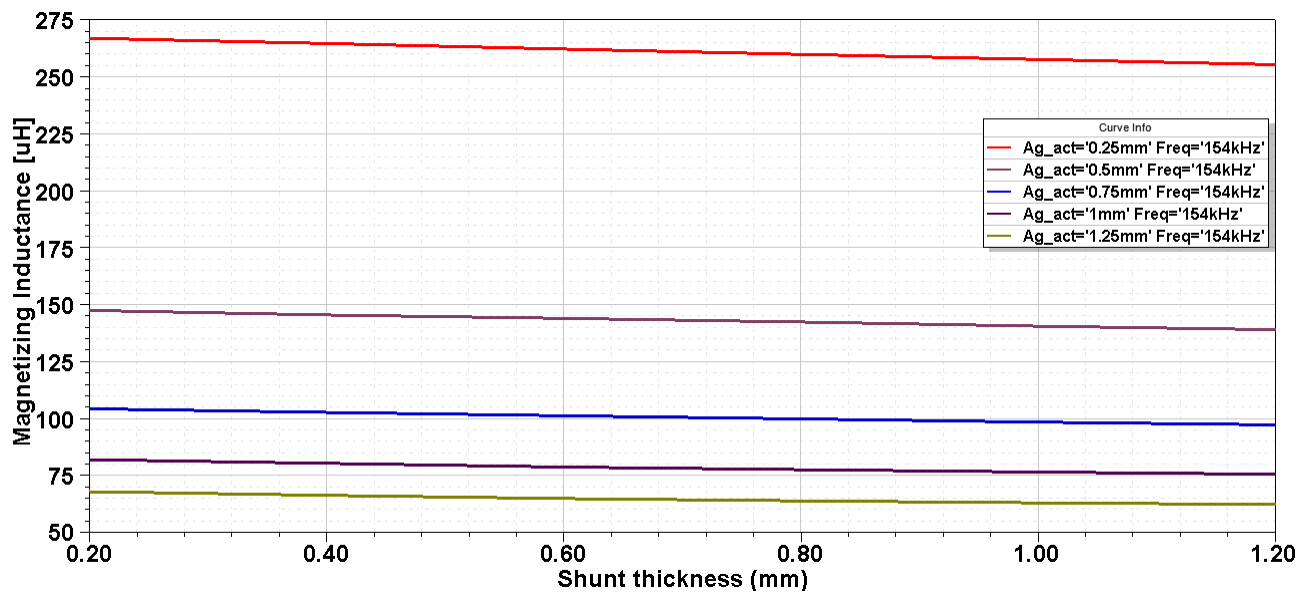
Figure 5.11 Conductor thickness verification



(a)



(b)



(c)

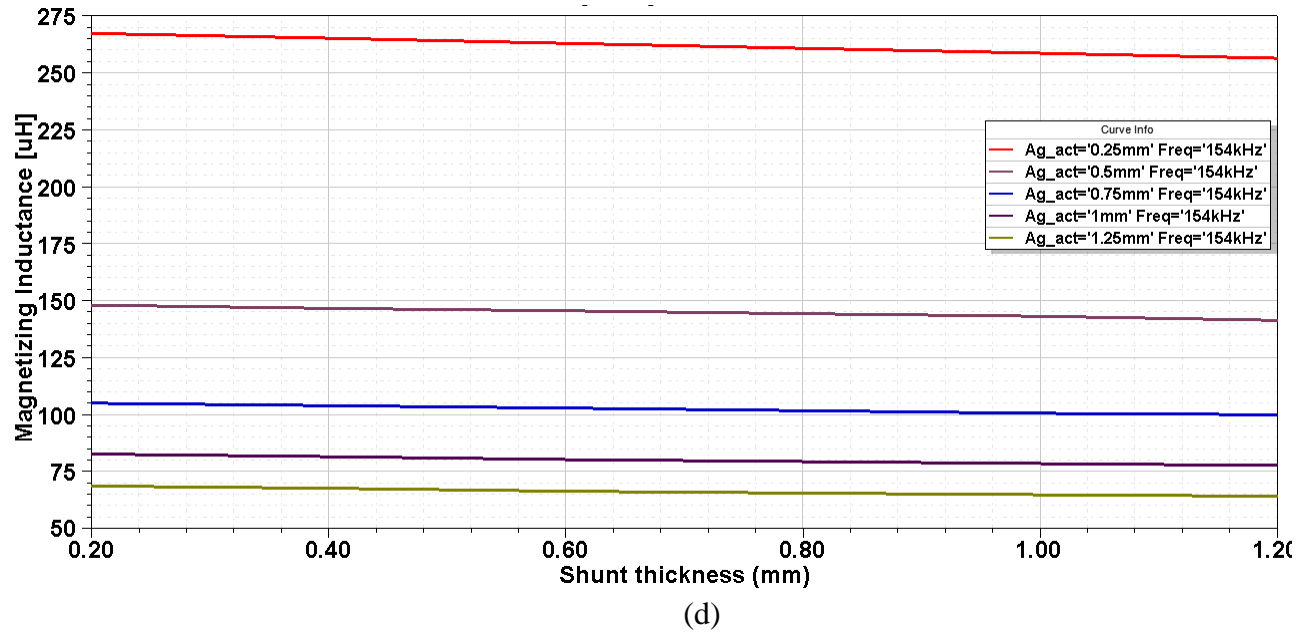


Figure 5.12 Magnetizing inductance for different permeability (a) 100, (b) 50, (c) 150 and (d) 200.

In order to determine the shunt thickness and its permeability, the leakage inductance is plotted for various shunt thickness at different permeability as shown in Fig. 5.13. The airgap length is fixed as 0.75mm. It can be observed that the required value of leakage inductance is achievable with the shunt layers of permeability 200 and 250 and shunt thickness in range of 0.6 to 0.8mm. The optimum permeability and thickness are determined next.

To determine the optimum permeability, copper losses are plotted against shunt thickness for various permeability as shown in Fig. 5.14. From the plot, the copper losses are minimum when both the shunt thickness and permeability of material are minimum. Based on the results, it is obtained as 0.75mm shunt thickness and permeability of 200.

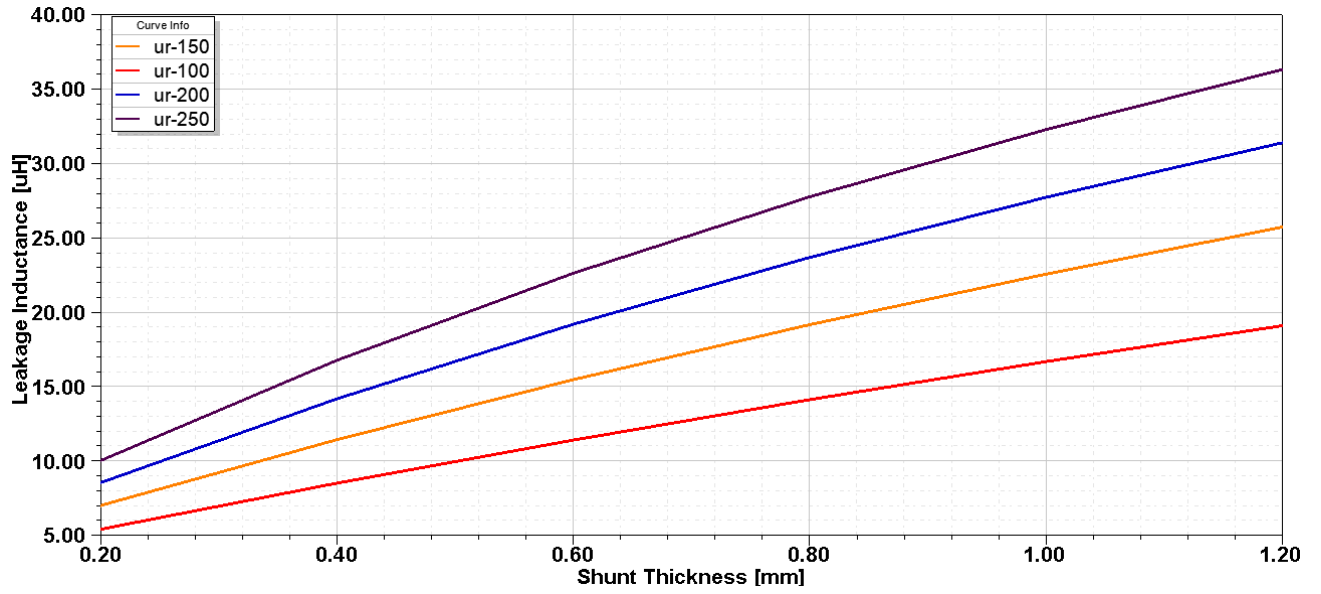


Figure 5.13 Leakage inductance at various permeability.

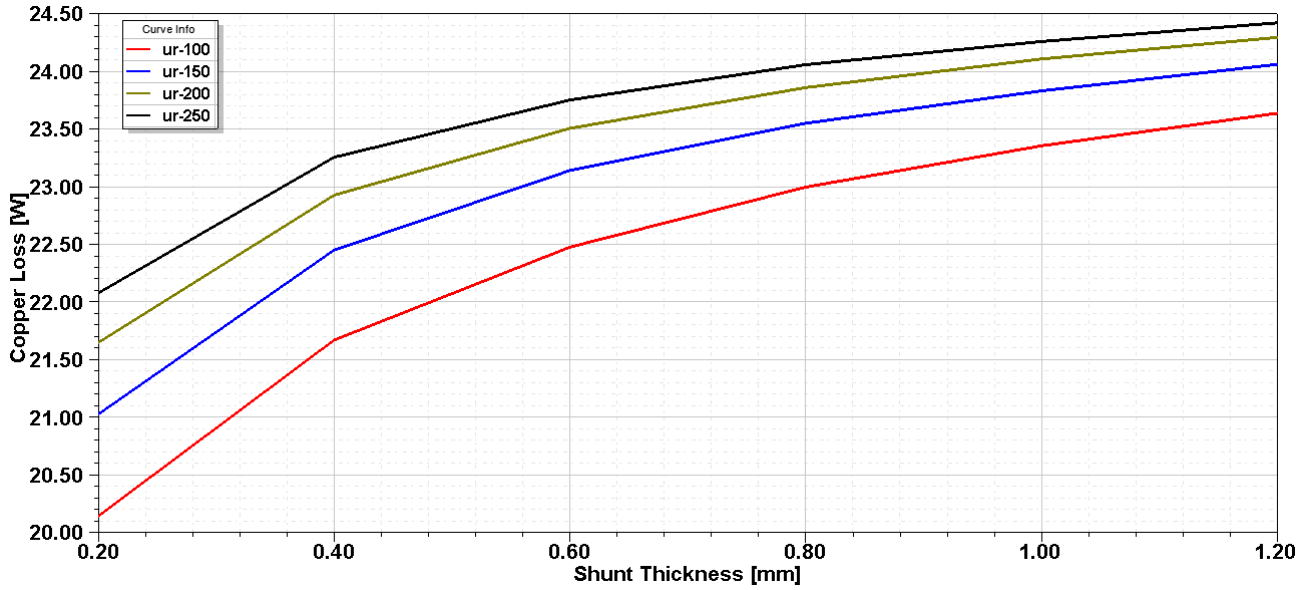


Figure 5.14 Copper loss vs shunt thickness for various permeability.

The results of final design are shown in Table 5.4. The simulations are performed in 3D FEA to confirm the results. Though there is increase in copper loss due to the introduction of magnetic shunt, the increased loss is within the maximum loss limit.

Table 5.4 Final design result comparison

Parameters	Spec	Analytical results	Simulation result 2D	Simulation result 3D
Magnetizing Inductance L_m (μH)	100	100.4	101.0	102
Leakage Inductance L_{lk} (μH)	22	2.44	22.6	23.4
Core Loss (W)	-	2.55	1.47	1.57
Copper Loss (W)	-	41.2	23.8	25.46
Total Loss (W)	< 30	43.75	25.27	27

CHAPTER 6

CONCLUSION AND FUTURE WORK

6.1 Summary

Planar transformer advantages over conventional transformer are discussed. Importance of magnetic integration are provided highlighting its advantages. The role of magnetics design in LLC converter application are briefed and how leakage inductance of transformer can be used as resonant inductor is discussed.

The complete design flow for an integrated transformer is provided in this thesis. The analytical equations needed for the design of a transformer are provided in detail.

An integrated planar transformer has been designed for LLC Converter application with the help of provided design equations. The effects behind high frequency eddy current loss are discussed. The windings of transformer are interleaved to reduce the losses. Then it is shown that the thickness of the conductor cannot be determined based on skin depth and also shown the optimum thickness varies based on the design. The finite element simulation results are provided for all cases.

The methods to improve leakage inductance of transformer are discussed. The impact of leakage inductance with a magnetic leakage layer is shown. The design is suitably modified and provided optimum magnetic layer thickness with improved leakage inductance provided losses are maintained within the requirement to avoid overheating of transformer.

6.2 Future Work

The interleaving of windings introduces extra insulation between the winding layers which may increase parasitic capacitance of transformer. Studies can be performed in future to calculate the parasitic capacitance and to mitigate the capacitance if required. Some LLC converter system may require integration of capacitor along with the transformer, in such a case this study can be put to use to improve the parasitic capacitance of transformer to make complete integration of resonant components.

REFERENCES

- [1] McLyman, C. (1988). *Transformer and inductor design handbook* (2nd ed., rev. and expanded.. ed., Electrical engineering and electronics. 49). New York: Dekker.
- [2] C. Quinn, K. Rinne, T. O'Donnell, M. Duffy and C. O. Mathuna, "A review of planar magnetic Techniques and technologies", Applied Power Electronics Conference (APEC), vol. 2, pp. 1175-1138, 2001
- [3] Hurley, W., Wölfle, Werner H, Ebrary, Inc, & Wiley InterScience. (2013). *Transformers and inductors for power electronics: Theory, design and applications*.
- [4] N. Dai, A. W. Lotfi, G. Skutt, W. Tabisz, F. C. Lee, "A comparative study of high frequency low profile planar transformer technologies", Applied Power Electronics Conference (APEC), vol. 1, pp. 226-232, 1994
- [5] MAGNETICS: Designing with Planar Ferrite Cores (Technical Bulletin) <http://www.mag-inc.com> [Mar.12 ,2018]
- [6] Kumar S, Shinde T, Vasambekar P. Engineering high permeability: Mn-Zn and Ni-Zn ferrites. Int J Appl Ceram Technol. 2015; 12:851-859
- [7] J. S. Ngoua Teu Magambo et al., "Planar Magnetic Components in More Electric Aircraft: Review of Technology and Key Parameters for DC–DC Power Electronic Converter," in IEEE Transactions on Transportation Electrification, vol. 3, no. 4, pp. 831-842, Dec. 2017.
- [8] T. R. Gunewardena, "Manufacturing design considerations for planar magnetics," Proceedings: Electrical Insulation Conference and Electrical Manufacturing and Coil Winding Conference, Rosemont, IL, 1997, pp. 309-311. doi: 10.1109/EEIC.1997.651114
- [9] C. Ropoteanu, N.-D. Codreanu, C. Ionescu, "Thermal investigation of a planar core power transformer", Proc. 39th Int. Spring Seminar Electron. Technol. (ISSE), pp. 112-115, May 2016

- [10] R. Severns and G. Bloom, *Modern DC-TO-DC switch mode power converter circuits*, V. N. Reinhold, 1st Edition, 1985, pp. 321-324
- [11] G. E. Bloom and R. Severns, "The generalized use of integrated magnetics and zero-ripple techniques in switchmode power converters," 1984 IEEE Power Electronics Specialists Conference, Gaithersburg, MD, USA, 1984, pp. 15-33. doi: 10.1109/PESC.1984.7083459
- [12] Z. Ouyang, G. Sen, O. C. Thomsen and M. A. E. Andersen, "Analysis and Design of Fully Integrated Planar Magnetics for Primary-Parallel Isolated Boost Converter," in IEEE Transactions on Industrial Electronics, vol. 60, no. 2, pp. 494-508, Feb. 2013. doi: 10.1109/TIE.2012.2186777
- [13] A. Kats, G. Ivensky and S. Ben-Yaakov, "Application of integrated magnetics in resonant converters," Proceedings of APEC 97 - Applied Power Electronics Conference, Atlanta, GA, 1997, pp. 925-930 vol.2. doi: 10.1109/APEC.1997.575756
- [14] Z. Ouyang, O. C. Thomsen, M. A. E. Andersen and T. Björklund, "Low profile, low cost, new geometry integrated inductors," 2011 Twenty-Sixth Annual IEEE Applied Power Electronics Conference and Exposition (APEC), Fort Worth, TX, 2011, pp. 150-156. doi: 10.1109/APEC.2011.5744589
- [15] D. Beatty and I. Batarseh, "Topical overview of soft-switching PWM high frequency converters," Southcon/95. Conference Record, Fort Lauderdale, FL, 1995, pp. 47-52. doi: 10.1109/SOUTHC.1995.516076
- [16] G. Hua and F. C. Lee, "An overview of soft-switching techniques for PWM converters," EPE J., vol. 3, no. 1, Mar. 1993.
- [17] B. Yang, "Topology investigation for front end DC/DC power conversion for distributed power systems," Ph.D. dissertation, Center Power Electron. Syst., Virginia Tech, Blacksburg, 2003.
- [18] V. Belevitch, "The lateral skin effect in a flat conductor" Philips tech. Rev. 32 (6/7,18), 221-231, 1971

- [19] W. A. Roshen, "High-Frequency Tunneling Magnetic Loss in Soft Ferrites," in IEEE Transactions on Magnetics, vol. 43, no. 3, pp. 968-973, March 2007. doi: 10.1109/TMAG.2006.882750
- [20] M. N. O. Sadiku, "A simple introduction to finite element analysis of electromagnetic problems," in IEEE Transactions on Education, vol. 32, no. 2, pp. 85-93, May 1989. doi: 10.1109/13.28037
- [21] M. A. Saket, N. Shafiei and M. Ordonez, "LLC Converters With Planar Transformers: Issues and Mitigation," in IEEE Transactions on Power Electronics, vol. 32, no. 6, pp. 4524-4542, June 2017. doi: 10.1109/TPEL.2016.2602360
- [22] J. Zhang, W. G. Hurley and W. H. Wolfle, "Gapped transformer design methodology and implementation for LLC resonant converters," in Proc. IEEE Appl. Power Electron. Conf. Expo., 2014, pp. 726-731
- [23] Z. Ouyang, O. C. Thomsen and M. A. E. Andersen, "The analysis and comparison of leakage inductance in different winding arrangements for planar transformer," 2009 International Conference on Power Electronics and Drive Systems (PEDS), Taipei, 2009, pp. 1143-1148. doi: 10.1109/PEDS.2009.5385844
- [24] W. G. Hurley and D. J. Wilcox, "Calculation of leakage inductance in transformer windings," in IEEE Transactions on Power Electronics, vol. 9, no. 1, pp. 121-126, Jan 1994. doi: 10.1109/63.285502
- [25] M. Li, Z. Ouyang, B. Zhao and M. A. E. Andersen, "Analysis and modeling of integrated magnetics for LLC resonant converters," IECON 2017 - 43rd Annual Conference of the IEEE Industrial Electronics Society, Beijing, 2017, pp. 834-839. doi: 10.1109/IECON.2017.8216144
- [26] J. Zhang, Z. Ouyang, M. C. Duffy, M. A. E. Andersen and W. G. Hurley, "Leakage Inductance Calculation for Planar Transformers With a Magnetic Shunt," in IEEE Transactions on Industry Applications, vol. 50, no. 6, pp. 4107-4112, Nov.-Dec. 2014. doi: 10.1109/TIA.2014.2322140

- [27] Y. Liu, “High Efficiency Optimization of LLC Resonant Converter for Wide Load Range”, Master thesis, Virginia Polytechnic Institute and State University: Blacksburg, Virginia, 2007.
- [28] DMR95- Material Datasheet.(www.chinadmegc.com) [Oct.10, 2017]

BIOGRAPHICAL SKETCH

Vigneshwaran Gurusamy was born in Tamil Nadu, India. He received B.Tech degree in electrical and electronics engineering from SASTRA University, Thanjavur, India in 2012. From 2012 to 2016 he was an Engineer in Computer Aided Engineering group with focus on electrical machine design at Lucas-TVS, an auto electrical company in Chennai, India. Since 2016, he has been with the Power Electronics and Drives Laboratory at UT Dallas. His research interests include fault diagnosis of electrical machines and design of electromechanical devices like electrical machines and medium frequency transformers.

CURRICULUM VITAE

VIGNESHWARAN GURUSAMY

Academic History

The University of Texas at Dallas, Richardson, TX

Master of Science in Electrical Engineering

May 2018

SASTRA University, Thanjavur, Tamil Nadu, India

Bachelor of Technology in Electrical and Electronics Engineering

May 2012

Research Experience

Erik Jonsson School of Engineering and Computer Science, The University of Texas at Dallas

Power Electronics and Drives Laboratory

November 2016- Present

- Design of Integrated Planar transformer for LLC converters.
- Development of TI Webench model and documentation for TI PMLK experiment kits of Buck, Boost and Buck-Boost converters.
- Development of system model for Inter turn short circuit fault analysis of Permanent Magnet Synchronous motor.

School of Electrical and Electronics Engineering, SASTRA University

High Voltage Laboratory

December 2011- May 2012

- Experimental Investigation on various faults in single phase and three phase transformers.
- Impulse testing of transformers and analysis of data.

Professional Experience

Advanced Engineering, Lucas-TVS, Chennai, India

Development Engineer in CAE team

July 2012 – July 2016

- Responsible for design of various electrical machines like claw pole alternators and motors, Permanent magnet synchronous motors, BLDC motors for automotive and traction applications.
- Development of performance prediction methodology for field-oriented control of synchronous motors including effect of battery resistance.

Publications

- Yuan Qi, Emine Bostanci, **Vigneshwaran Gurusamy**, Bilal Akin, “A Comprehensive Analysis of Short Circuit Current Behavior in PMSM Inter Turn Short Circuit Faults”, *Early access article in IEEE Transaction on Power Electronics*, DOI: 10.1109/TPEL.2018.2809668

Honors & Awards

- Research Assistant Scholarship, Spring 2018, The University of Texas at Dallas.
- Recipient of Merit award in Lucas-TVS ,2015.
- Dean’s list ,2009, SASTRA University.